Comparative Analysis of Human Color Vision Diversity: Spatiotemporal Dynamics of Attention-Related Neural Activity Toward Color Saliency

髙橋, 直子

Comparative Analysis of Human Color Vision Diversity: *Spatiotemporal Dynamics of Attention-Related Neural Activity Toward Color Saliency*

ヒトの色覚多様性の比較研究：
色顕著性に関連する注意の神経活動の時空間ダイナミクス

九州大学

Naoko Takahashi
髙橋　直子

Supervisor: Dr. Chihiro Hiramatsu

Kyushu University
Graduate School of Design

This dissertation is submitted for the degree of
Doctor of Philosophy

March 2025

Acknowledgements

I would like to express my deepest gratitude to my supervisor, Associate Professor Chihiro Hiramatsu, for her unwavering support throughout my master's and PhD studies. Her passion and curiosity for our field have been a constant source of inspiration. I am incredibly grateful for her patience and generosity, without which I could not have completed this work.

I am also deeply thankful to Professors Yuki Motomura, Masataka Sawayama, Hiroshige Takeichi, Satoru Miyauchi, and Satoshi Nakadomari. Their intellectual guidance, insightful discussions, and encouragement have been invaluable in shaping and strengthening my research. I am incredibly honored to have learned from each of them.

Special thanks to Professor Gerard B. Remijn and Professor Hiroshige Takeichi for their thorough scrutiny and insightful comments as reviewers of this dissertation.

My sincere appreciation goes to Tamotsu Eguchi and Kozue Fujisawa for their advice and support during my time as a RIKEN student researcher and part-time assistant. I am equally thankful to Professor Hiroshige Takeichi for his additional guidance and encouragement during this time. I also extend my sincere thanks to Professor Satoru Miyauchi for his invaluable expertise in EEG experimentation, which provided me with essential skills and research insights.

I sincerely appreciate all study participants for their time and invaluable cooperation.

To my friends and lab members, both current and past, I am truly grateful for their support and camaraderie. Their presence has made this journey more meaningful and enjoyable, even on the most challenging days.

I also want to express my heartfelt gratitude to Chanprapha Phuangsuwan and Chanida Saksirikosol from Rajamangala University of Technology Thanyaburi for their friendship and unwavering support. The memories we shared are filled with joy and never fail to bring a smile to my face.

My academic journey at Geiko began in Oi Lab, where I spent a foundational period as a research student. I am deeply grateful for the opportunity to have been part of the lab and for Professor Naoyuki Oi's insightful guidance and support, which helped lay the groundwork for my research direction in graduate study.

I would also like to express my sincere gratitude to the faculty members at the Design Human Science Course for providing me with the foundational knowledge essential to my research. Over the years, many of them have not only guided me academically but also offered various forms of support. Their kindness and encouragement have meant a great deal to me throughout my graduate study.

Above all, I am deeply grateful to my family for their unwavering love, encouragement, and sacrifices. Their faith in me has been my greatest strength, and your constant support has carried me through every challenge. This dissertation is as much yours as it is mine.

In loving memory of my mother and my grandparents.

Abstract

Color perception is a fundamental aspect of human sensory experience, yet it varies significantly across individuals due to genetic and physiological diversity in the visual system. Most humans are trichromats, perceiving colors through three classes of cone cells with sensitivities that generally align with predictions based on opponent-processing models. However, minority color vision phenotypes often deviate from the predictions, demonstrating enhanced color sensitivity that differs from typical trichromats and suggesting unique processing mechanisms. The precise neural and perceptual mechanisms behind this enhanced sensitivity remain elusive. Given the role of colors as versatile navigation and communication tools, accurately assessing sensory differences and similarities across color vision types is essential to deepening our understanding of the perceptual characteristics and underlying mechanisms for both typical and minority phenotypes.

This dissertation investigates how variations in cone sensitivity influence both neural activity and behavioral performances across different color vision types. Specifically, it examines how neural responses reflect differences in color saliency by analyzing the broad spatiotemporal characteristics of event-related potentials (ERPs) in both typical and anomalous trichromats. Two target stimuli (red and blue-green) were chosen to create different levels of saliency during a discrimination task from a common non-target stimulus (green), allowing comparison of perceived saliency across color vision types. Although the chromatic properties of these stimuli remained constant, their perceived saliency was reversed between the color vision types, enabling direct comparison of neural and behavioral responses. This

approach also simulates real-world conditions, where individuals rely on consistent physical light properties to perceive colors without chromatic adjustments.

Using electroencephalography (EEG) to record ERPs during an attention-demanding oddball task, this study examines how attentional resources are modulated by chromatic stimuli with varied saliency. The analysis includes both categorical distinctions and continuous chromatic sensitivity differences to address individual variability within groups, particularly in anomalous trichromats, where traditional categorical analyses might otherwise mask subtle within-group variations. A linear mixed-effects model was applied to both behavioral and neural data to explore how continuous variations in chromatic sensitivity shape perceptual and neural responses.

The findings revealed both shared and distinct characteristics of behavioral and neural processing across color vision types. For typical trichromats, both behavioral and neural responses consistently reflected saliency differences, aligning with expectations based on their sensory characteristics. Specifically, reaction times (RTs) were generally faster for the more salient red stimulus, and the spatiotemporal ERP analyses revealed faster, stronger, and more spatially widespread activation for the red stimulus. In contrast, anomalous trichromats did not show a distinct neural response pattern when comparing the two target stimuli. However, when each target was compared to the common non-target green stimulus, anomalous trichromats showed a faster neural response to the more salient blue-green stimulus, confirming the expected saliency difference. Although both color vision types demonstrated faster neural response to their respective more salient target stimuli, the spatiotemporal ERP pattern between groups were not markedly different.

RT analysis indicated that continuous chromatic sensitivity provided a better fit compared to categorical distinction, highlighting nuanced sensory variations reflected in behavioral performance. While the overall RT patterns suggested the influence of reduced chromatic sensitivity of anomalous trichromats, RT patterns did not support reversal saliency relation-

ship, indicating a more complex relationship between chromatic sensitivity and behavioral responses.

These results highlight the robust sensitivity of typical trichromats along the red-green axis, while anomalous trichromats exhibited more nuanced responses to saliency, reflecting complex relationships between their chromatic sensitivities and corresponding behavioral and neural responses. Although both color vision types responded faster to their respective more salient target stimuli, suggesting shared processing mechanisms, anomalous trichromats showed more ambiguity in response to saliency differences. This ambiguity may suggest the presence of enhanced perceptual mechanisms, though the specifics remain unconfirmed. To verify the contribution of such mechanisms, further research with larger sample sizes is necessary to confirm and extend these findings.

Table of contents

List of figures

List of tables

List of Publications and Presentations

The parts of this thesis have been presented or published in scientific venues:

- **Journal Article**: [Temporal and spatial analysis of event-related potentials in response to color saliency differences among various color vision types.], [Frontiers in Human Neuroscience], [2024]. DOI: https://doi.org/10.3389/fnhum.2024.1441380.
- **Conference Presentation**: [Diversity in neural activity toward varying color saliency in relation to attention among individuals with different color vision types.], [Vision Society of Japan], [2023]. Related to Chapter 2 and Chapter 3.
- **Poster Presentation**: [Color saliency and attention change represented by neural processing in individuals with various color visions.], [Vision Sciences Society Annual Meeting], [2022]. DOI: https://doi.org/10.1167/jov.22.14.3445. Related to Chapter 2 and Chapter 3.

Nomenclature

Units

μV	microvolt
cd/m^2	candela per square meter
$k\Omega$	kilo-ohm
deg	degree
Hz	Hertz
K	Kelvin (Unit used to express color temperature)
mn	millisecond
nm	nanometer

Acronyms

AIC	Akaike Information Criterion (a method for model selection based on information theory)
BIC	Bayesian Information Criterion (a similar approach to AIC, incorporating Bayesian principles)
CAD	Color Assessment and Diagnosis (name of a color vision test)
CIE	Commission Internationale de l'Éclairage (International Commission on Illumination)

CIs Confidence Intervals

D65 D65 (A standard light that simulates natural daylight with a color temperature of about 6,500 K [kelvin], which is similar to the color of the sky at noon on a clear day)

EEG Electroencephalography

ERPs Event-Related Rotentials

fMRI Functional Magnetic Resonance Imaging

ICs Independent Components

IT Inferotemporal Cortex

LGN Lateral Geniculate Nucleus

LME Linear Mixed-Effects

MEG Magnetoencephalography

RT Reaction Times

SE Standard Error

SSVEPs Steady-State Visual Evoked Potentials

Chapter 1

Introduction to Human Color Vision—Rise of Trichromacy

Human color perception exhibits inherent diversity, with minority phenotypes exhibiting shifts in cone sensitivities at the retinal level. These shifts lead to difference in color discrimination compared to typical trichromatic color vision. However, the perceptual characteristics among minority phenotypes do not always align with estimations based solely on the spectral sensitivities. The mechanisms behind these variations, particularly from a neural perspective, remain insufficiently understood.

This study investigates the spatiotemporal characteristics of event-related potentials (ERPs) in response to color stimuli with varying saliency. This chapter begins with providing an overview of the evolutionary background of human color vision and the mechanisms that underlie its diversity. It also reviews the current understanding of perceptual variations, highlighting gaps in the knowledge, especially in relation to typical color vision. The chapter concludes with the research objectives and an outline of the dissertation's overall structure.

1.1 The Evolutionary Background of Trichromatic Vision

Human color vision, like that of other species, evolved through mutations and natural selection. While human vision is predominantly trichromatic, early ancestors had different visual systems. More than 540 million years ago, early vertebrates are believed to have been tetrachromatic, possessing four types of cone cells, including one sensitive to ultraviolet (UV) light (Bowmaker, 1998; Jacobs, 2012; Lamb et al., 2007).

Around 200 million years ago, early mammals transitioned to a predominantly nocturnal lifestyle, which led to the loss of two of these photopigments—those sensitive to UV and middle wavelengths——since color vision likely became less critical in low-light environments. This adaptation resulted in dichromatic vision, with sensitivity primarily to short and long wavelengths region on the visible spectrum (Borges et al., 2018; Xian-Guang et al., 2002).

Approximately 25 million years ago, during the evolution of Old World primates, gene duplication occurred within the long-wavelength (L) cone (Hunt et al., 1998; Jacobs, 2009; Nathans et al., 1986). This gave rise to a new middle-wavelength (M) cone. Combined with the short-wavelength (S) cone, this enabled the emergence of trichromatic vision among apes, human ancestors, Old World monkeys and some of New World monkeys. Trichromacy allowed for better discrimination of red-green color differences and is believed to have provided adaptive advantages in tasks such as foraging, mate selection, social signals, and navigation of complex environments (Hiramatsu et al., 2017; Kawamura, 2016).

However, the advantages of trichromacy over dichromacy are not universally clear. Some studies suggest that dichromats may be more effective at detecting certain visual cues, such as bluish fruit in low light or from a distance (Caine et al., 2010; Melin et al., 2007, 2014). Conversely, other research has shown no significant difference in fruit detection efficiency

between dichromats and trichromats in spider monkeys (Hiramatsu et al., 2009), illustrating the complexity of color vision across different contexts.

1.2 Human Color Vision, Polymorphism, and Neural Mechanism

Humans typically have trichromatic vision, which is mediated by three classes of cone cells——L-, M-, and S-cones——with peak sensitivities around 565 , 535 nm, and 420 nm, respectively (Nathans et al., 1986; Stockman et al., 1993). Although each cone cell is sensitive to a specific part of the light spectrum, their spectral ranges overlap, enabling a more nuanced color experience by allowing comparisons between the stimulation levels of different cones.

The primary neural mechanism for color perception involves color-opponent neurons, which contrast signals from different cones to enable color discrimination. Red-green perception is primarily driven by the contrast in stimulation between L- and M-cones. Blue-yellow perception, in contrast, arises from the combination of S-cone input with a joint response from L-cone and M-cone responses (Li et al., 2022; Sakurai and Mullen, 2006). These two cardinal-axes of color discrimination enable trichromats to perceive color in a three-dimensional space. The spectral distribution of each cone provides essential chromatic information, meaning that any spectral shift in their spectral sensitivity directly impacts an individual's ability to discriminate along these color axes.

Polymorphism is a key characteristics of human color vision, with most being trichromatic while some exhibit variations in spectral sensitivity, particularly in the L- and M-cones. This variation stems from the genetic similarity and proximity of the L- and M-opsin genes (Neitz

and Neitz, 2011). These genes are located side by side on the X-chromosome, and share about 96% of their amino acid sequences (Nathans et al., 1986) because M-cone opsin originated from a gene duplication of the L-cone opsin. This similarity often leads to genetic recombination, causing shifts in spectral sensitivity (Deeb, 2005). For example, a shift in the L-cone sensitivity toward middle wavelengths results in protanomalous trichromacy, while a shift in the M-cone sensitivity toward longer wavelengths results in deuteranomalous trichromacy.

In some cases, recombination can lead to the complete replacement of one type of cone by the other, resulting in dichromacy. Protanopia occurs when the L-cone is replaced by an M-like cone, while deuteranopia results when the M-cone is replaced by an L-like cone. These color vision deficiencies are more common in males due to the X-linked inheritance pattern of the L- and M-opsin genes. Approximately 8% of males of European descent exhibit some form of color vision deficiency, while the prevalence among females is much lower, around 0.04% (Tait and Carroll, 2009). Figure 1.1 show cases of dichromacy with different spectral characteristics.

Interestingly, a significant proportion of females (about 12$\sim$15%) are carriers of genes that influence L- and M-cone variability (Jordan et al., 2010; Tait and Carroll, 2009). These cases are considered to have a potential for tetrachromatic vision, where an individual has four spectrally distinct types of cones. While most carriers do not exhibit tetrachromacy, there has been at least one observed case of a female with a fourth spectral sensitivity (Jordan et al., 2010; Jordan and Mollon, 2019). The full impact of tetrachromacy on color perception is still under investigation.

This genetic variation in human color vision reflects the evolutionary and biological diversity within our species. While trichromacy is often viewed as having provided adaptive advantages, the presence of polymorphisms has been maintained throughout evolution. The contemporary role of color perception may differ from the early human evolution, and it

remains unclear how much adaptive values the full range of color vision continues to offer as our environment and lifestyle change. Further research into these variations may help clarify how these phenotypes function and what advantages they might offer in varying contexts.

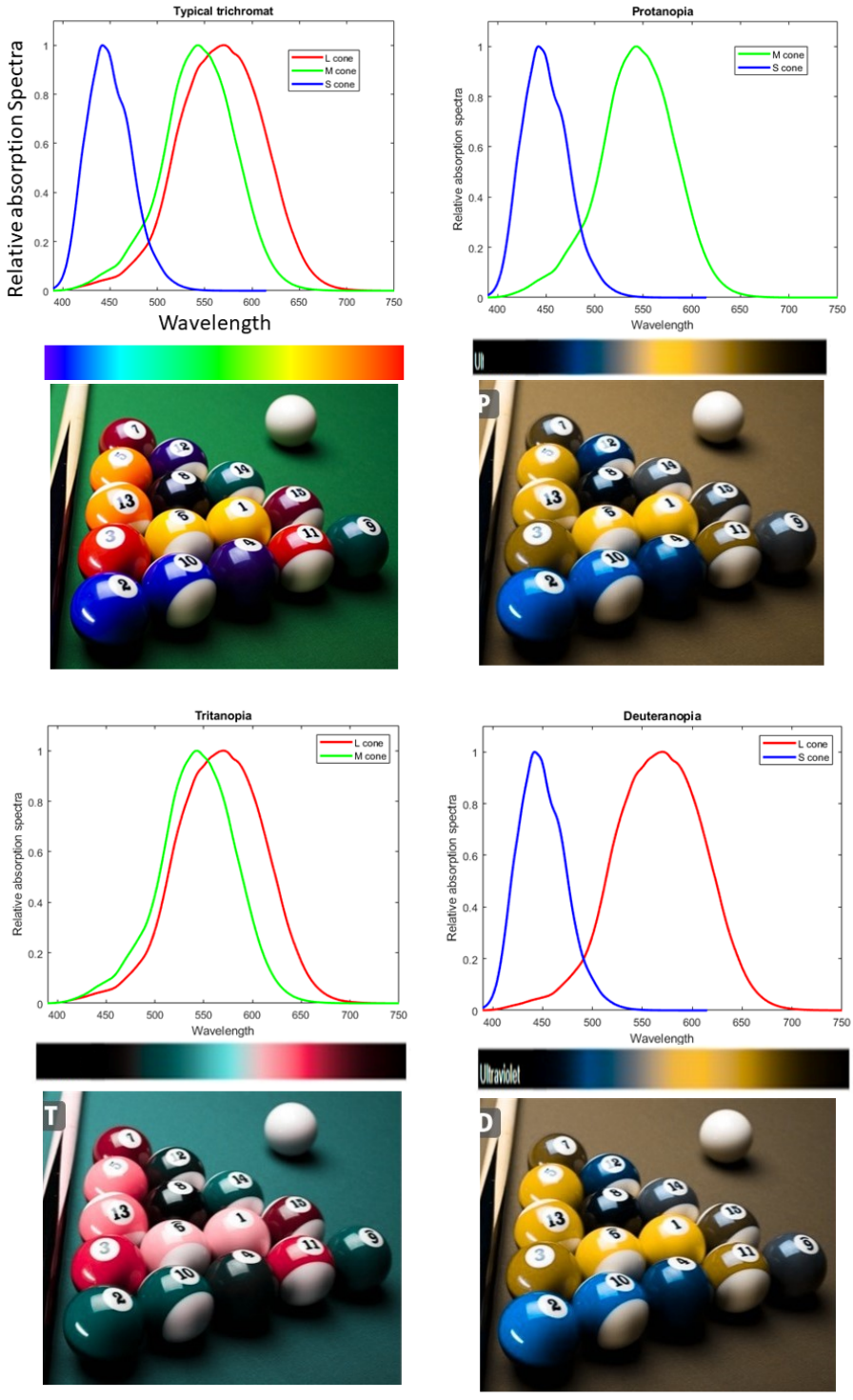

Fig. 1.1 Spectral sensitivity of cone responses across different color vision types, based on 2-deg cone fundamentals (Stockman and Sharpe, 2000). The spectral color bar in the middle and sample images at the bottom simulate protanopic, deuteranopic, and tritanopic vision, created using the Chromatic Vision Simulator application. Each simulated distribution illustrates a form of dichromatic color vision, each with unique cone sensitivity characteristics. While dichromatic vision is relatively rare, anomalous trichromats, whose spectral sensitivities partially shift toward another cone type, retain all three cone classes. This partial deviation results in reduced color discrimination within specific spectral ranges.

1.3 Color Perception of Minority Phenotypes

For individuals with minority color vision phenotypes, their perception is considered to reflect the sensitivity characteristics of their cones. The absence of sensitivity within a specific spectral range generally results in reduced color discrimination, effectively compressing perceived color space from three- to two-dimensions. For dichromats, this reduction indicates the absence of red-green discrimination, leaving color discrimination to rely solely on blue-yellow contrast.

In case of anomalous trichromats, the situation is more complex, as their color perception depends on the degree of spectral shift between L- and M-cone. This shift can vary from 1 to 12 nm across anomalous trichromats (Asenjo et al., 1994; Merbs and Nathans, 1992; Neitz and Neitz, 2011). In general, the closer the L- and M-cone sensitivity are to each other, the less perceptually distinct the red-green contrast becomes.

Although the disadvantages of these variations are often highlighted, some studies suggest advantages for dichromats in humans, such as the ability to detect objects camouflaged by color (Mollon, 1989; Morgan et al., 1992; Pastilha et al., 2019; Troscianko et al., 2017) and detecting temporally high-frequency target visual stimuli (Sharpe et al., 2006), and contrast sensitivity in achromatic conditions (Janáky et al., 2014).

1.4 Neural Mechanisms and EEG Studies

1.4.1 Neural Mechanisms of Color Vision

Visual information processing begins in the retina, where light is absorbed by photosensitive cone cells. While some initial processing, such as the color opponent mechanism, occurs in the retina, most visual signal processing takes place in the cortex.

Signals from the retina travel through the lateral geniculate nucleus (LGN) to the primary visual cortex (V1). These areas show color-opponent responses and luminance contrast sensitivity, similarly to the retina. Early areas like LGN and V1 exhibit retinotopy, preserving spatial correspondence with the visual field. Central vision (foveal vision) benefits from a disproportionately large cortical representation, enabling higher resolution and more precise color perception due to the dense population of cone cells (Liu and Wandell, 2005; Wandell and Winawer, 2011).

Signals related to object feature recognition follow the ventral visual pathway in monkeys:

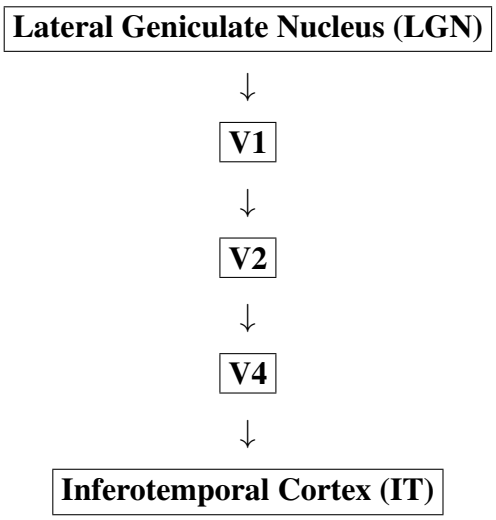

The ventral pathway processes basic visual features, such as edges, contours, and color, along with the more complex attributes like shapes and object identity. In contrast, spatial and motion-related features are processed in the separate dorsal pathway (Fang and He, 2005; Ingle et al., 1982; Kravitz et al., 2013; Mishkin et al., 1983; Rousselet et al., 2004).

As signals travel along the ventral pathway, neural responses become increasingly specialized. For instance, neurons in V4 and IT exhibit heightened selectivity for specific colors, even distinguishing the same hue under varying luminance contrasts (Namima et al., 2014). This forms the neural basis for categorical color perception. While higher cortical regions also exhibit retinotopic organization, spatial correspondence to the visual field diminishes as processing becomes more abstract. This enables the integration of different visual attributes like edges, contours, shapes, and colors into coherent object representations. Figure 1.2 illustrates the processing streams of visual inputs in the macaque monkey, highlighting the ventral and dorsal pathways as well as the different cortical regions in the visual cortex.

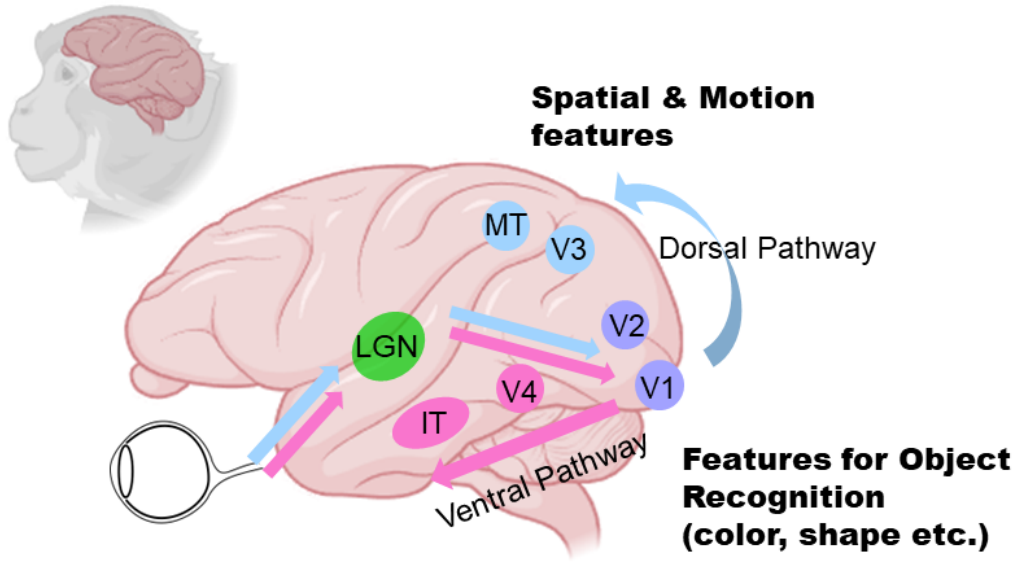

(a) Schematic diagram of visual pathways in the macaque brain.

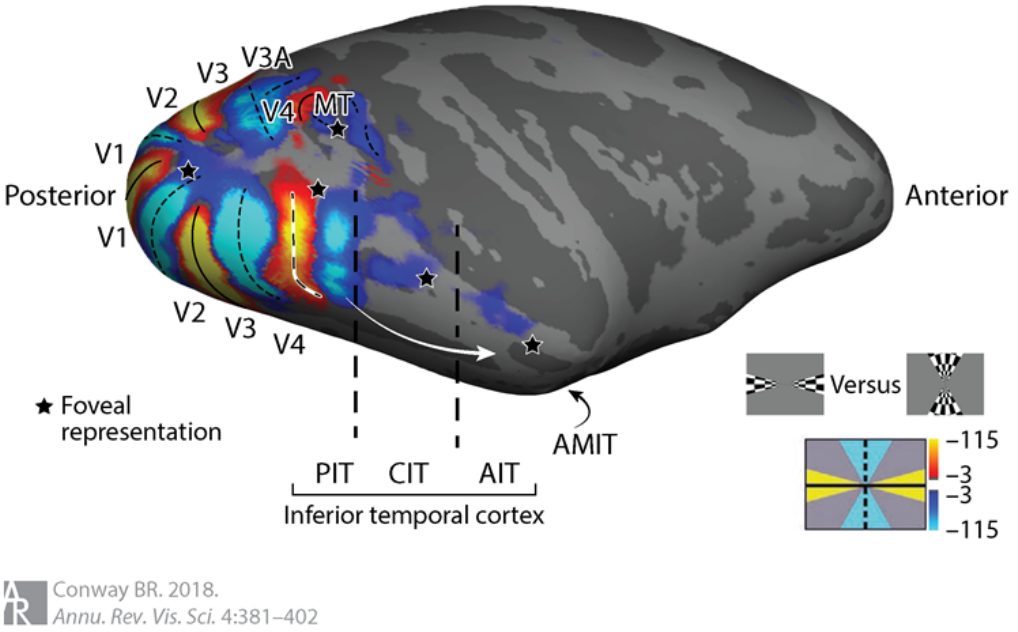

(b) fMRI representation of visual fields in the macaque brain, adapted from Conway (2018).

Fig. 1.2 (a) Schematic of visual pathways showing ventral and dorsal streams in the macaque brain. The signals are further processed in higher-order mechanisms in distinct pathways: the ventral and dorsal pathways. The ventral pathway, often referred to as "what" pathway, processes visual information related to object recognition, such as color and shapes. In contrast, the dorsal pathway, or where/how pathway, handles luminance information and motor-related signals, supporting spatial resolution. Brain illustration adapted from bioBlender (bioblender.eu). License: CC BY-NC-SA. (b) fMRI data illustrating early visual field representations (V1, V2, V3, etc.) in the macaque cortex.

1.4.2 Advances in Human Neuroimaging

Historically, research on visual processing relied on animal models, such as cats, mice, and non-human primates (e.g., macaques), due to ethical considerations in human studies (Hubel and Wiesel, 1977; Maunsell et al., 1999; Reinagel et al., 1999). While these animal studies provided foundational insights, human studies were largely limited to observations of brain injuries.

Recent advances in non-invasive brain imaging technologies— such as electroencephalography (EEG), Magnetencephalography (MEG), and functional magnetic resonance imaging (fMRI)—have enabled researchers to study the correspondence between cortical responses and visual stimuli with minimal burden on human participants, unveiling the complexities of human visual processing (Kastner et al., 2006; Mullen et al., 2010).

EEG measures the brain's electrical activity by detecting voltage changes at the scalp, primarily reflecting postsynaptic potentials generated by cortical pyramidal cells near the scalp surface (Kirschstein and Köhling, 2009).

- ***Action Potentials*** are rapid voltage changes across a neuron's membrane, enabling direct communication between cells. However, their highly localized and transient nature causes them to cancel out in adjacent neurons, making them undetectable by EEG.
- ***Postsynaptic Potentials*** are graded voltage changes occurring in postsynaptic neurons when neurotransmitters bind to receptors. These signals aggregate across populations of neurons, creating electrical fields detectable by EEG.

EEG excels in capturing postsynaptic potentials with millisecond-scale temporal resolution. However, its spatial resolution is limited due to volume conduction, where electrical signals spread through the surrounding tissue and scalp surface. Despite these constrains, EEG is highly effective for investigating the timing and progression of neural processes (Bucci and Galderisi, 2011; Luck, 2014).

1.4.3 EEG Studies on Color Perception

Temporal dynamics in EEG recordings are often analyzed through event-related potentials (ERPs), which represent transient neural responses to stimulus perception. ERPs are computed by averaging voltage changes from stimulus onset across multiple trials. This averaging enhances the signal-to-noise ratio, isolating stimulus-related neural activity while minimizing unrelated fluctuations. Prominent waveforms in ERPs are interpreted as reflections of underlying stimulus processing mechanisms (Gefen, 2004; Luck, 2014).

Color perception has been studied extensively using attention-based tasks (Hillyard and Münte, 1984; Kuniecki et al., 2015). Harter and Aine (1984) proposed a model of selective attention, suggesting that attending to specific stimulus features modulates the neural activity of populations specialized in processing those features. For example, attention to color stimuli activates neurons concentrated in V4. Studies have identified characteristic ERP waveforms in response to color stimuli using discrimination or detection tasks. For example, a larger positive peak is observed between 120 to 230 ms post-stimulus at frontal to centro-parietal electrodes (Aine and Harter, 1986; Eimer, 1997) , followed by a negative peak between 200 to 320 ms post-stimulus. This negative peak is often interpreted as an attention-orienting process toward relevant stimulus features (Näätänen and Gaillard, 1983). Beyond these early components, a large positive peak, known as P3, emerges beyond 300 ms post-stimulus, reflecting attentional effects during post-perceptual processing (Eimer, 1997).

Studies on categorical color perception have revealed faster sensory processing for between-category stimuli. This is evidenced by shorter latencies in early components (e.g., P1 and N1) and larger amplitudes in later components (e.g., P2 and P3), suggesting enhanced processing for stimuli with categorical differences (Holmes et al., 2009). Steady-state visual evoked potentials (SSVEPs) further highlight early-stage preferences for intermediate hues (e.g., lime and magenta), indicating the complexity of early cortical color processing mechanisms (Kaneko et al., 2020). These findings underscore the utility of EEG in exploring both the temporal dynamics and cortical mechanisms of color vision, advancing our understanding of human perception. It is important to note that these studies are based on participants with typical trichromatic color vision.

1.5 Currently Known Perception of Minority Phenotypes

Despite the known limitations in red-green sensitivity, predicting discrimination sensitivity in minority phenotypes based solely on cone sensitivities remains a challenge. Current estimates of discrimination sensitivity often fail to align with experimental findings. For example, higher-than-expected red-green sensitivity has been reported in a range of studies, including psychophysical color-matching experiments and color-naming tasks involving cognitive components (Bosten, 2019; Moreira et al., 2021). For instance, dichromats have demonstrated color categorization abilities similar to typical trichromats when stimuli are presented with sufficient size and time for identification (Montag, 1994).

Various studies have attempted to explain this supra-threshold sensitivity. Some have suggested that rod cells may provide an alternative signal, contributing to color perception under certain conditions (Montag and Boynton, 1987; Nagy and Boynton, 1979; Smith and Pokorny, 1977). Other studies suggested that enhanced S-cone sensitivity in the long-wavelength region may serve as an alternative signal (Kurtenbach et al., 1999; Scheibner and

Boynton, 1968), or that variations in optical density could account for improved sensitivity (Neitz et al., 1999; Thomas et al., 2011).

Recent research also pointed to post-receptoral neural modulation as contributor to the perceptual enhancement in anomalous color vision types. For instance, a psychophysical study has suggested that post-receptoral enhancement plays a key role in boosting discrimination sensitivity (Boehm et al., 2021). Additionally, amplification of visually evoked potentials was recorded for binocular conditions (Rabin et al., 2018) and fMRI studies have documented amplified neural activity in the early visual cortex (V2) in cases of anomalous trichromacy, even during simple fixation tasks (Tregillus et al., 2021).

Overall, the prevailing evidence implies that a variety of mechanisms contribute to the extended sensitivity observed in both anomalous trichromacy and dichromacy. Nevertheless, a comprehensive understanding of this phenomenon remains elusive. Particularly, research linking perceptual and cognitive diversity with neural diversity is still scarce, highlighting a gap in the understanding of how neural mechanisms support these perceptual variations.

1.6 Experimental Design intent

The task design for this study was guided by the need to balance difficulty across typical trichromats and anomalous trichromats while using chromatically consistent stimuli and addressing the unique demands of ERP experiments on color vision phenotypes.

1. **Balanced Task Difficulty:**

   The goal of this study is to design tasks with varying levels of saliency for both color vision groups: typical trichromats and anomalous trichromats. Both more and less

salient targets were introduced to balance task difficulty and enable the assessment of neural and behavioral responses across groups using identical stimuli. This approach minimizes group-specific biases and allows for meaningful comparisons.

2. **Rationale for Using an Oddball Task:**

   The oddball task, widely-used paradigm in EEG studies, was selected to analyze attention effects. This is particularly relevant because ERP studies on color vision phenotypes are limited, and a straightforward paradigm aids in interpreting neural responses to saliency differences. By focusing on responses to infrequent deviant stimuli, the design helps uncover saliency-related neural mechanisms in color perception.

   To reduce confounding variables, the task was kept simple, with two target conditions presented in separate blocks and requiring a single response button. This simplicity ensured that:

   - Participants, particularly anomalous trichromats, could fully engage with the task without undue difficulty.
   - Attention remained centered on the stimuli rather than on task complexity, such as multi-button responses.

3. **Ensuring Comparable Difficulty Across Groups:**

   A key challenge was maintaining comparable task difficulty for both groups using identical chromatic stimuli. Adjusting stimuli based on individual chromatic sensitivities was avoided to prevent introducing extrinsic individual variability that could complicate group comparisons. Instead, the design prioritized consistent chromatic conditions, allowing analysis of how individual differences in sensitivity manifest in neural and behavioral performance.

4. **Task Simplicity and Fairness:**

   The target conditions were designed to be sufficiently detectable to ensure participants

could perceive the stimuli, while maintaining a level of difficulty necessary to elicit neural activity reflective of attentional load. Undetectable stimuli would have prevented the evaluation of neural and behavioral performance, defeating the study's purpose. By ensuring that both target conditions were within a detectable range, the study minimized task-related frustration and allowed for fair participation by all groups, regardless of color vision phenotype.

5. **Consideration for Minority Phenotypes:**
   Participants with minority phenotypes, such as anomalous trichromats, may approach color detection tasks with heightened caution due to their unique color perception experiences. To accommodate this, the task was designed to be fair and accessible to all participants without favoring one group over another. Conditions were created to ensure that each group had both easier and more difficult tasks, balancing performance expectations and avoiding biased interpretations.

6. **Avoiding Bias in Stimulus Design:**
   Care was taken to avoid conditions that might inherently favor one group over the other. For example:

   - Studies indicate that anomalous trichromats exhibit faster reaction times (RT) with blue-green stimuli compared to typical trichromats, reflecting higher saliency for this color range (Sunaga et al., 2013).
   - Conversely, during oddball tasks, early-phase ERP components and RTs show longer latencies for blue-green stimuli among typical trichromats, indicating lower saliency for such stimuli (Holmes et al., 2009).

   Based on these findings, blue-green stimuli were chosen as relatively more salient for anomalous trichromats and less salient for typical trichromats. This design aimed to balance task conditions while maintaining fairness and validity in performance evaluations.

1.7 Chromatic Space and Stimulus Selection

In this study, the stimuli were chosen based on the color space. The CIE (Commission Internationale de l'Éclairage) is an international standardization body specializing in light, lighting, vision, and colorimetry. This section reviews the historical development of the CIE color system and introduces the foundational concepts of uniform color space (Schanda, 2007).

1.7.1 Historical Basis: Color Matching Experiments

The CIE color system is built upon the additive color model (RGB color model) (Figure Figure 1.3), where any color light can be reproduced by combining red, green, and blue light in varying intensities. This principle, known as the color matching principle, forms the foundation for today's colorimetry. It can be expressed mathematically as:

$$C = R + G + B$$

Here, C represents the test light, which R,G, and B are the red, green, and blue primaries, also known as primary colors or primary stimuli and = indicates color matching between the test light and the mixed lights.

The definition of RGB primaries originates from independent color matching experiments conducted by William David Wright and John Guild in 1920s. In these experiments, participants were shown a test light and asked to adjust the intensities of three primary lights

(red, green, and blue) to match its color. A critical criterion for these primary colors was independence, meaning that no primary lights could be reproduced by mixing the other two.

The CIE adopted the results of these experiments, averaging the outcomes to define the concept of *"the CIE standard observer"*, a theoretical model representing human color perception. This standard observer became a foundation for the CIE 1931 color space (Fairman et al., 1997; Hunt and Pointer, 1985; Shaw and Fairchild, 2002).

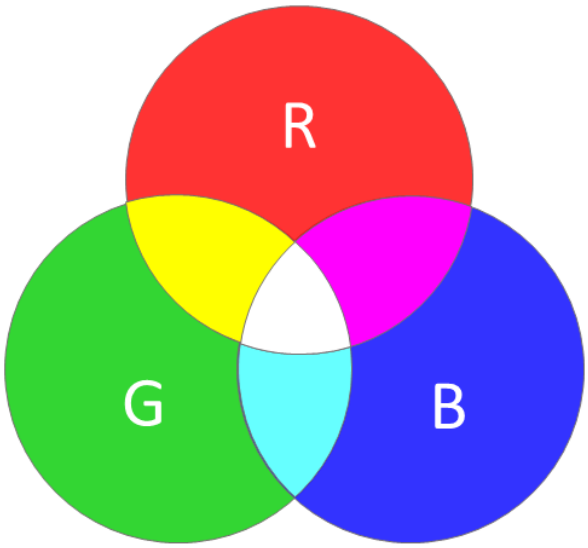

Fig. 1.3 Additive color mixture model, which forms the basis of colorimetry in the CIE color system. It explains how colors are perceived by combining different primary colors of light, which are red, green, and blue.

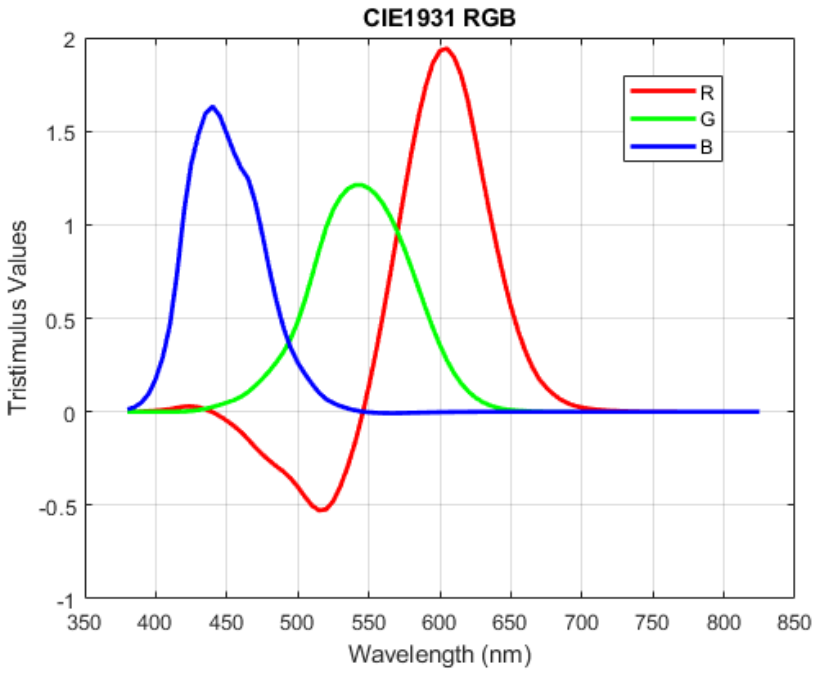

Fig. 1.4 CIE1931 RGB tristimulus values.

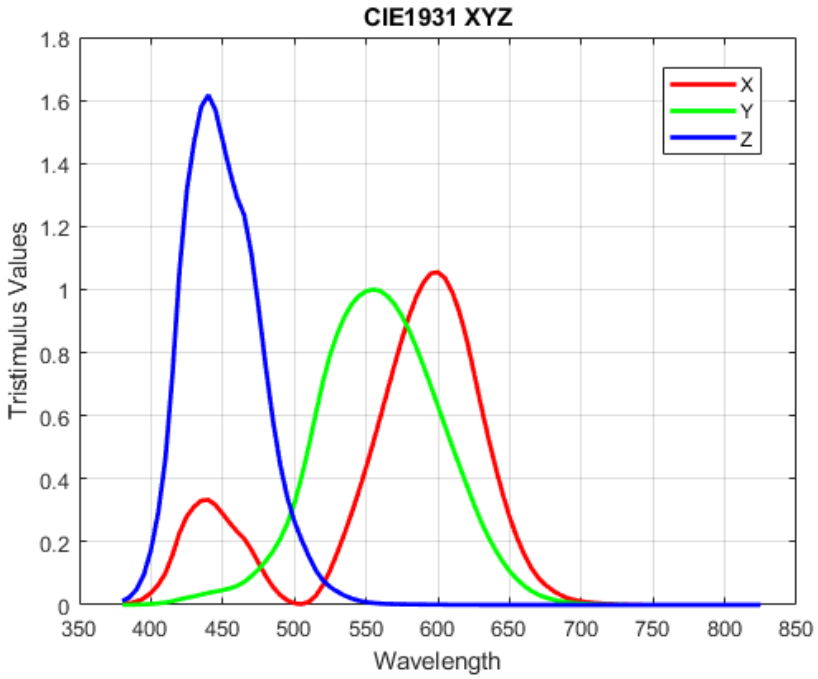

Fig. 1.5 CIE1931 XYZ tristimulus values.

1.7.2 Addressing Subtractive Adjustments

During the color matching experiments, some test colors required participants to subtract light from one of the primaries (e.g., red) to achieve a match (Figure 1.4). This subtraction was accomplished by adding one primary to test light to cancel out the excess intensity. This subtractive adjustment arose because the RGB primaries used in the experiments were highly saturated, making it impossible to represent all colors purely through additive combinations (Smith and Guild, 1931).

While this approach worked in the experimental setting, it introduced computational challenges, as negative light intensities are not physically meaningful. To overcome this, the CIE introduced a new set of mathematically transformed primaries, known as the X, Y, and Z values. These are linear combinations of the original RGB values, ensuring that all colors can be represented through additive combinations with only positive values (Figure 1.5).

1.7.3 Transition to Chromaticity Coordinates

Building on the X, Y, and Z system, the CIE derived xy chromaticity coordinates, which describe colors in terms of chromaticity (hue and saturation) independent of luminance (Figure 1.6). These chromaticity coordinates are calculated as follows:

$$x = \frac{X}{X+Y+Z}$$

$$y = \frac{Y}{X+Y+Z}$$

Note that Y value represents brightness value, though it is not equivalent to luminance, whereas x and y represents the chromaticity of the color.

The x and y coordinates provide a two-dimensional representation of the visible color spectrum, simplifying the visualization and comparison of color relationships (Ohno, 2000).

1.7.4 Uniform Color Space: CIE1976 u',v' uniform chromaticity scale diagram

While XYZ color space and xy chromaticity coordinates provide a framework for describing colors, they do not account for perceptual uniformity. In other words, the distances in these spaces do not correspond to the chromatic differences perceived by human observers. To address this limitation, CIE1976 u', v' uniform chromaticity scale coordinates were developed (Isbell, 1964; Mahy et al., 1994), based on the work of David L. MacAdam.

David L. MacAdam, a researcher at Eastman Kodak, conducted extensive color matching experiments to study perceptual differences in color represented in xy coordinates. Using 25 reference colors, a single participant was asked to indicate the range of color indistinguishable from reference color. These ranges were represented as ellipses, now known as MacAdam ellipses, centered on each reference point. The study, repeated over 25,000 trials, demonstrated that the size and shape of these ellipses vary across the color space, highlighting perceptual non-uniformity (Kaarna et al., 2002; MacAdam, 1942; Wundheiler, 1945).

To create a more uniform color space, the u'v' chromaticity coordinates were derived by transforming the xy chromaticity diagram (Figure 1.6). This transformation standardized the sizes of the MacAdam ellipses, making them more circular and equal in size. The u'v' coordinates are calculated as follows:

$$u' = \frac{4x}{-2x+12y+3} = \frac{4X}{X+15Y+3Z}, \quad v' = \frac{9y}{-2x+12y+3} = \frac{9Y}{X+15Y+3Z}$$

The u'v' uniform color space provides a more perceptually accurate representation of chromatic differences, making it a valuable tool for studies involving human color perception (Melgosa et al., 1994; Pointer, 1981). However, it is important to note that while the inconsistency in the sizes of ellipses were reduced, they were not perfectly consistent. Variables in ellipse size remain particularly in the peripheral region of the color space, which must be considered carefully when using it.

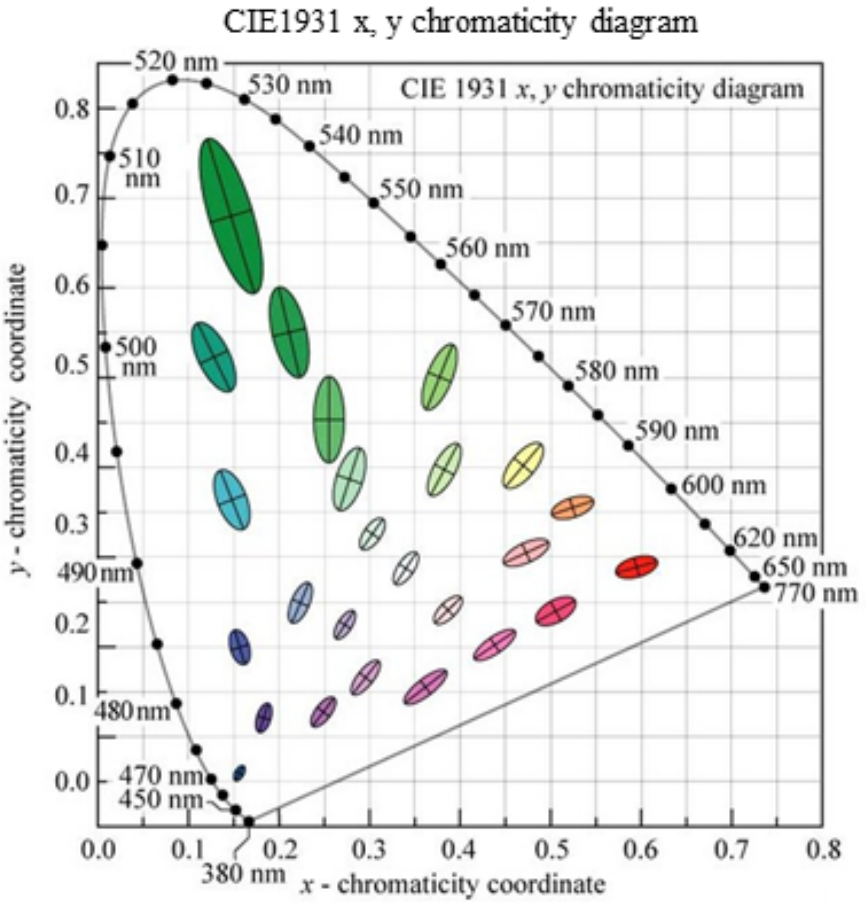

Fig. 1.6 CIE1931 x,y chromaticity diagram plotted with MacAdam ellipses. The CIE1931 x,y chromaticity diagram (commonly known as the CIE1931 xy diagram or color space) is a foundational chromaticity diagram representing human perceptual color space. Figure adapted from Mokrzycki and Tatol (2011).

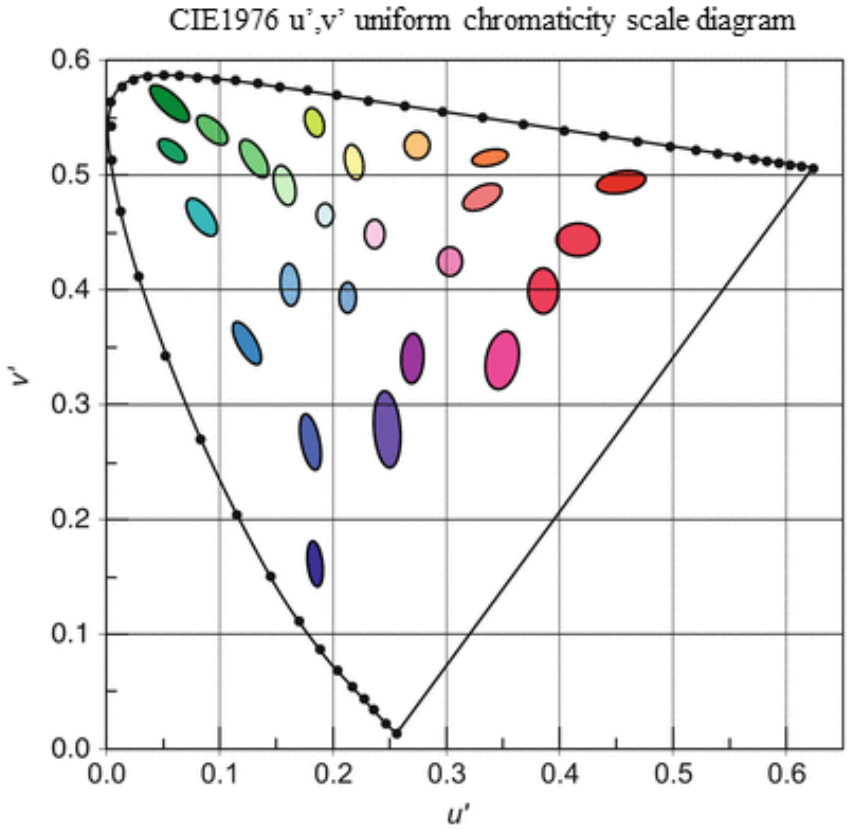

Fig. 1.7 CIE1976 u',v' uniform chromaticity scale diagram with MacAdam ellipses. The CIE1976 u',v' uniform chromaticity scale diagram (commonly referred to as the CIE1976 u',v' diagram or color space) is one of the uniform color spaces standardized by the CIE. It is a perceptually uniform color space based on Wundheiler (1945). The size of the ellipses becomes more inconsistent as saturation increases, indicating reduced uniformity in the color space. Figure adapted from Schanda (2016).

1.8 Equiluminance Among Stimuli

In this study, all the color stimuli were adjusted to have equal luminance to the background to avoid luminance difference from serving as alternative cues during the detection task. Equiluminance was measured using flicker photometry (or heterochromatic flicker photometry), a standard psychophysical method for quantitively adjusting differences in photopic luminance, which relies on inputs from cone cells. This section explains the basis of the method and the neural mechanisms behind its use for achieving luminance equality.

In flicker photometry, two colored lights (a test color and reference color) are alternated rapidly, typically at 10 to 20 Hz (Lee et al., 1988; Pokorny et al., 1989). Participants adjust the luminance of the test light, either increasing or decreasing its intensity, to identify the point where the sensation of flicker is minimized. At this point, the luminance of the test light is considered to match that of the reference light.

1.8.1 Visual Pathways and Contrast Sensitivity

The effectiveness of flicker photometry relies on differences in the processing characteristics of luminance and motion contrast compared to chromatic contrast. Luminance and motion contrast exhibit high temporal and spatial sensitivity, while chromatic contrast is relatively low in both temporal and spatial resolution. These differences arise from the distinct neural pathways that process these visual features (Denison et al., 2014; Kastner et al., 2006).

Motion-related spatial features rely on luminance contrast, primarily derived from inputs from L- and M-cones. This information is processed through the magnocellular layers of the

lateral geniculate nucleus (LGN), which are highly sensitive to rapid changes in luminance contrast across adjacent visual field. This sensitivity underlies the perception of motion, where temporal sensitivity is critical. On the other hand, chromatic signals are relayed to separate layer called parvocellular layers, which exhibit lower temporal resolution compared to the magnocellular layers.

Motion-related visual features are subsequently processed along the dorsal pathway, while chromatic contrasts are processed in the ventral pathway. This reflects their functional specialization for motion and color perception, respectively.

1.8.2 Luminance Detection in Flicker Photometry

In flicker photometry, the luminance levels of two colors are adjusted to achieve luminance equality. When the luminance levels of two colors are mismatched, participants perceive a strong flicker due to the high temporal sensitivity. When the luminance levels are matched, the flicker sensation diminishes because the magnocellular system no longer detects differences in luminance contrast.

1.9 Research purpose and Scope

The primary objective of this research is to deepen our understanding of how variations in cone sensitivity influence neural activity and behavioral responses in individuals with different color vision phenotypes. While it is known that inherent diversity in cone sensitivities leads to variations in color perception, the mechanism that bridges these differences——particularly at the neural level——remain elusive. Existing research suggests that the perceptual gap

between individuals with typical and anomalous color vision is not solely a function of cone sensitivity but driven by a combination of perceptual enhancement mechanisms, presumably both at receptoral and post-receptoral stages. However, how these broader mechanisms interact and are reflected in neural signals has not been fully explored.

This study aims to identify both the distinguishing and shared spatiotemporal characteristics of neural activity among different color vision phenotypes during attention-demanding tasks. Using EEG to record event-related potentials (ERPs), the research examines how attentional resources are modulated by differences in color saliency among individuals with different color vision types. Through this investigation, the study seeks to provide more comprehensive insights into the neural process underlying color perception diversity, with a particular focus on the modulation of attention in response to chromatic stimuli.

1.10 Novelty of This Research

A main novelty of this research lies in the use of chromatically identical stimuli across all participants, regardless of their varying chromatic sensitivities. Instead of adjusting stimuli to ensure consistent perceived saliency differences for each participant, the same chromatic conditions were used. This approach allowed for the analysis of how neural activity reflects spatiotemporal characteristics of ERPs and behavioral responses in a manner that reflects real-world conditions, where the physical properties of light remain fixed despite individual differences in color perception. However, the luminance of the stimuli was individually adjusted to ensure that stimulus detection was based on chromatic differences rather than luminance cues.

Another unique feature of this study is the use of an attention-demanding paradigm to evoke saliency-related neural activity across a broad spatiotemporal scale. Attentional

mechanisms enhance the processing of critical visual features, such as chromatic contrasts, which serve as key cues for efficient and timely action planning in daily tasks. By adopting an attention-driven approach, the influence of attentional modulation on perceptual and cognitive performance could be effectively examined across individuals with varying chromatic sensitivities. This method not only enables the investigation for early visual areas but also extends to other cortical regions potentially involved in the extended perceptual sensitivity observed in minority color vision phenotypes, an area where knowledge remains limited. This highlights the dynamic neural and behavioral variation across different color vision types.

A further novel approach lies in the symemetrically reversed saliency relationships within the stimuli, where a stimulus that is more salient to typical trichromats is less salient to individuals with minority color vision phenotypes and vice versa. This design enabled us to capture how attentional modulation and neural processing differ across color vision types without adjusting chromatic conditions.

Moreover, our study considers not only categorical differences between color vision types (e.g., typical trichromats vs. anomalous trichromats) but also accounts for continuous variability in color sensitivity within participants, particularly among those with minority color vision phenotypes. When focusing solely on categorical distinctions, the variability within the category often becomes noise in the data. To address this, a linear mixed-effect model was used to account for continuous sensitivity differences, providing a more nuanced understanding of how these variations influence neural and behavioral responses.

1.11 Overview of the dissertation structure

This dissertation is organized into four main chapters, followed by an appendix that includes additional results:

- **Chapter 2: Materials and Methods** This chapter provides a detailed description of the study design and methodology. It includes sections on participant profiles, stimulus design, task procedures, and experimental apparatus. Additionally, it outlines the behavioral and EEG data analysis methods, including the linear mixed-effect models used for both behavioral and ERP analyses.
- **Chapter 3: Results** The third chapter presents the findings from the study. It begins with the results of the flicker photometry task, followed by behavioral results derived from the linear mixed-effect model analysis. The chapter also covers the ERP results, including both the model-based analysis on P3 component and exploratory spatiotemporal examination of neural activity using the cluster-based permutation analysis.
- **Chapter 4: Discussion and Conclusion** This chapter interprets the findings presented in Chapter 3, connecting them with existing literature and theoretical frameworks. The broader implications of the results are discussed, particularly with respect to the neural and perceptual mechanisms underlying color vision differences. The chapter concludes by summarizing key findings and offering potential directions for future research.
- **Appendix** The appendix contains supplementary results, focusing on individual-level analyses that provide additional insights into variability across participants.

Chapter 2

Materials and Methods

2.1 Participants

This study involves 19 male participants, all with normal or corrected-to-normal visual acuity. The majority were undergraduate and graduate students at Kyushu University School of Design (mean age $\pm$ standard deviation: 23.32 $\pm$ 2.68 years).

Males were exclusively selected in the study because approximately 12% of females carry variant red and green visual pigment genes, which can alter cone sensitivity. To prevent any unintended influence on color perception, females were excluded from participation (Jameson et al., 2014; Jordan et al., 2010).

To assess each participant's color vision type, four color vision tests were conducted: the Ishihara pseudoisochromatic plate test, the Color Assessment and Diagnosis (CAD) test (Barbur et al., 2021), the HMC anomaloscope (Oculus) (Melamud et al., 2004), and

the Farnsworth–Munsell 100 Hue Test (Verriest et al., 1982). Different color vision tests provide slightly different aspects of color perception due to different measurement methods, thus, color vision type was determined based on the combined results. Five participants were classified as deuteranomalous trichromats (with altered M-cone sensitivity), one as a deuteranope (lacking the M-cone), and the rest as typical trichromats.

All participants received financial compensation for their involvement. The study protocol was conducted in accordance with the Declaration of Helsinki and was approved by the Ethics Committee of the Graduate School of Design at Kyushu University (Approval No. 316). Written informed consent was obtained from each participant prior to the experiment.

Individual variations can be observed among typical trichromats, however, perceptual variation is particularly pronounced among minority color vision phenotypes. In order to account for these variations comprehensively beyond categorical differentiation of color vision types, red-green sensitivity was evaluated using the CAD test. Table 2.1 presents the red-green sensitivity thresholds of the deuteranomalous and deuteranope participants. These thresholds indicate the amount of saturation required to distinguish colors from a neutral gray point along the red-green axis, where a value of 1 represents the average discrimination ability of typical trichromats (Barbur and Rodriguez-Carmona, 2017; Barbur et al., 2021). For graphical images of individual results, see Appendix B.

In this study, the mean threshold for typical trichromats was 1.1 ± 0.2, while the mean threshold for anomalous trichromats was 13.1 ± 7.9.

Participant code	**Red-green threshold**	**Color vision type**
Participant 14	21.63	Deuteranomalous trichromacy
Participant 07	19.36	Deuteranopia
Participant 02	19.35	Deuteranomalous trichromacy
Participant 18	13.34	Deuteranomalous trichromacy
Participant 03	9.07	Deuteranomalous trichromacy
Participant 16	2.19	Deuteranomalous trichromacy

Table 2.1 Red-green thresholds assessed using the CAD test and identified color vision types based on the anomaloscope test for participants with minority color vision phenotypes. Participants are listed in descending order according to their red-green threshold.

Participant code	Red-green threshold	Color vision type
Participant 01	0.70	Typical trichromacy
Participant 04	1.20	Typical trichromacy
Participant 05	1.17	Typical trichromacy
Participant 06	1.02	Typical trichromacy
Participant 08	0.96	Typical trichromacy
Participant 09	1.21	Typical trichromacy
Participant 10	1.24	Typical trichromacy
Participant 11	0.89	Typical trichromacy
Participant 12	1.19	Typical trichromacy
Participant 13	1.15	Typical trichromacy
Participant 15	1.06	Typical trichromacy
Participant 17	0.93	Typical trichromacy
Participant 19	1.19	Typical trichromacy

Table 2.2 Red-green thresholds assessed using the CAD test and identified color vision types based on the anomaloscope test for typical trichromats. Participants are listed in ascending order according to the participant code.

2.1.1 CAD test

The CAD test is a relatively new color vision assessment tool, chosen for its ability to quantitatively and conveniently evaluate chromatic sensitivity. This facilitates direct comparisons of chromatic sensitivity among participants. Details on how the CAD test evaluates chromatic sensitivity are provided below.

The CAD test measures chromatic sensitivity along the cardinal color axes of the red-green and blue-yellow, assessing deviations in sensitivity involving L-cone, M-cone, and S-cone cells. Individuals with high chromatic contrast sensitivity can detect color differences with smaller contrasts, while those with deviations in sensitivity, such as dichromacy and anomalous trichromacy, require larger chromatic contrasts to perceive the color differences. The test uses chromatic stimuli from the red-green and blue-yellow axes to determine discrimination thresholds relative to the D65 neutral gray point, a standard illuminant representing daylight standardized by the CIE. This gray point marks the convergence of the two cardinal axes in CIE xy color space. In the CAD test, a threshold of 1 is defined as the mean chromatic sensitivity of typical trichromats, while higher thresholds indicate reduced chromatic sensitivity, requiring greater saturation for color perception.

During the assessment, participants detect a chromatic stimulus that moves diagonally and respond to which direction the stimulus moved in a four alternative forced-choice task. To ensure that participants rely on color differences rather than brightness cues during the detection task, the luminance of both the background and the stimulus is varied randomly as the stimulus moves across the display, resembling a mosaic. Figure 2.1 (a) and (b) shows a schematic display of the CAD test and candidate test stimuli, and Figure 2.1 (c) provides an example of CAD test results.

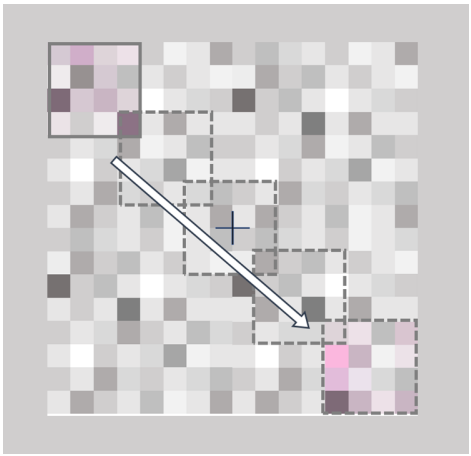

(a) CAD Test Display

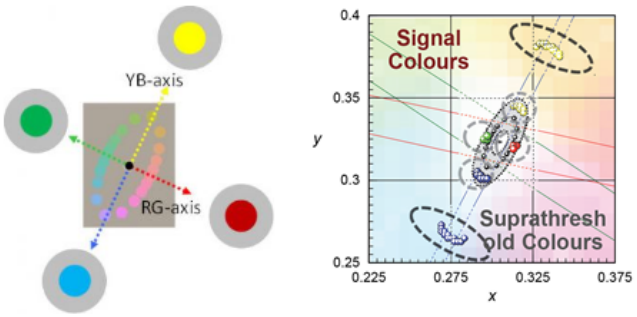

(b) CAD Stimulus Samples

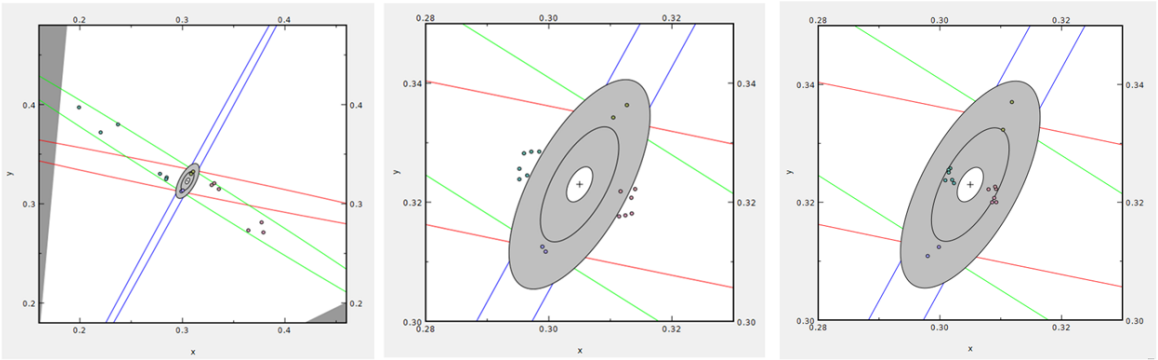

(c) Example outputs of the test

Fig. 2.1 (a) Stimulus image of the CAD test, showing a square-shaped stimulus moving from the top left to the bottom right. The stimulus window is filled with pixelated squares where luminance varies randomly, masking luminance effects during the detection task. (b) Sample stimulus candidates used in the test. Stimuli are randomly selected to test sensitivity along the red-green or blue-yellow axes during the test. The images are adopted from Barbur et al. (2021). (c) Example output of the test results. The left and middle panels show cases of deuteranomalous trichromacy with varying red-green sensitivities, while the right panel shows a typical trichromat result, where all dots, representing detection thresholds, are clustered around the inner circle, indicating average detection thresholds for typical trichromacy.

2.2 Stimulus

2.2.1 Stimulus Selection

The task involved three different chromatic stimuli, which were either assigned as target or non-target stimulus. These stimuli were selected to achieve varying levels of chromatic contrast when each stimulus was paired with a shared standard stimulus. The chromaticities of the stimuli were carefully chosen based on the u',v' diagram, which allows for the estimation of perceptual chromatic differences as Euclidean distances for individuals with typical trichromacy (Pointer, 1981). This color space represents perceptual chromatic differences geometrically, allowing a direct comparison between stimuli (Ohno, 2000).

Three specific colors—blue-green, red (with an orange tint), green—were selected, all equidistant from the D65 neutral gray in the u', v' diagram (Figure 2.2). Their specific coordinates were (0.1679, 0.4670) for blue-green, (0.2278, 0.4696) for red, and (0.1817, 0.4936) for green. Each was positioned uniformly 0.03 units from D65 (0.1978, 0.4683), ensuring consistent saturation relative to the neutral point. In the attention task, blue-green and red served as target (or deviant) stimuli, while green functioned as the standard (non-target).

In this uniform color space, perceptual differences between colors can be quantified through Euclidean distance (Ohno, 2000). The greater the distance between two points, the larger the perceptual difference. The Euclidean distances between blue-green and red from green were 0.03 and 0.052, respectively. Given that red is farther from green in this color space, it was expected to be more perceptually salient than blue-green. This is also reflected in categorical color distinctions: blue-green is categorically more similar to green than red is, which enhances the perceptual salience of red when contrasted with green. Studies on

color categories and their psychophysical effects indicate that categorical differences can lead to faster behavioral responses and earlier neural activations (Holmes et al., 2009; Witzel and Gegenfurtner, 2015). Hence, this chromatic arrangement was designed to evoke distinct levels of saliency, amplified by these categorical differences.

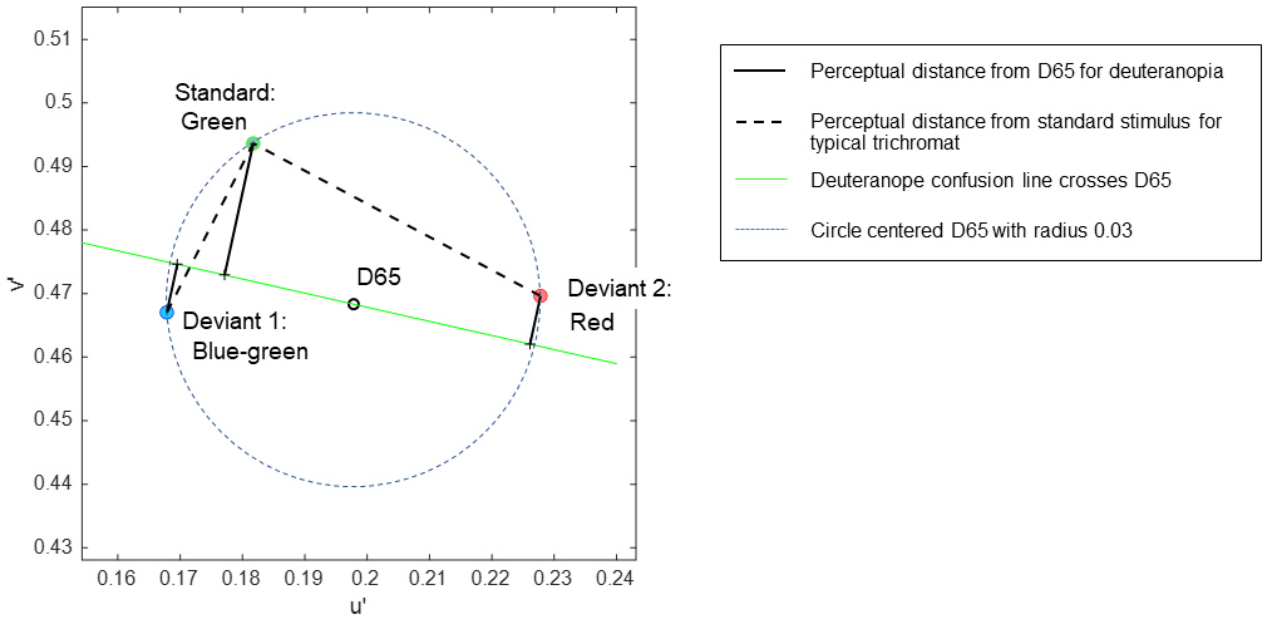

Fig. 2.2 The coordinates of stimuli in the CIE 1976 u', v' uniform chromaticity scale diagram, in which perceptual distance is represented as Euclidean distance for typical trichromats. The expected chromatic contrasts between the standard and deviant stimuli are represented as line lengths: black dotted lines represent typical trichromacy, and black solid lines represent deuteranopia.

2.2.2 Stimulus Comprehension for Minority Color Vision Phenotypes

Understanding chromatic differences in minority color vision phenotypes, such as deuteranopia, requires a careful approach due to their reduced two-dimensional color space, which results from the absence of specific cone sensitivities. In dichromacy, colors along the same confusion line—where all colors appear identical—are indistinguishable. These lines, originating from a single point called the "copunctal point", are unique to each type of minority color vision phenotype, depending on which cone cells deviate from those of typical trichromats.

Although the exact cardinal color axis for minority color vision phenotypes is still debated, it is generally estimated as perpendicular to the confusion line that intersects the D65 neutral gray (Broackes, 2010). As Pridmore (2014) notes, in dichromats, the empirical color axis is orthogonal to the confusion line, passing through the neutral gray point. Thus, chromatic distances for deuteranopia can be represented by the distance along this orthogonal axis (Figure 2.2).

Based on this assumption, the relative chromatic contrasts for deuteranopia were estimated from the perpendicular distances of the stimuli to the deuteranopic confusion line. These contrasts were 0.0290 for blue-green and 0.0134 for red, calculated from distances of 0.0212 for green, 0.0078 for blue-green, and 0.0078 for red. The confusion line intersecting D65 also serves as a categorical boundary (Broackes, 2010), where chromatic differences are calculated by summing or subtracting the orthogonal distances, depending on whether the stimuli are on opposite or the same sides of the line.

This predicts that for deuteranopes, blue-green would be more salient than red when contrasted with green, reversing the typical trichromat ratio (0.03/0.052 = 0.57 for trichromats vs. 0.029/0.0134 = 2.16 for deuteranopia). Despite variability in red-green thresholds among

individuals with anomalous trichromacy, the same chromatic stimuli were used for all participants to explore neural diversity under consistent visual input. Luminance contrast was controlled by adjusting all stimuli to 20 D65 using flicker photometry (see section 2.5 for the details).

2.3 Task Design

To investigate attentional response to chromatic contrasts, an oddball paradigm was employed, a widely used approach to elicit evoked potentials associated with attentional processing (Picton et al., 1992; Sutton et al., 1965). This paradigm presents a series of stimuli, with a frequently appearing standard stimulus interspersed with a rarely presented deviant stimulus in a pseudo-random order. Participants were instructed to detect the deviant and press a button as quickly as possible following its appearance (Figure 2.3).

A response button, which was a rectangular-shaped box that could be held in the hand, was connected to a trigger box, which in turn was directly linked to the EEG amplifier. Participants held the button during the task and submitted their response by pressing it with their thumb. This setup ensured precise recording of participant reactions and allowed for real-time synchronization with the neural data being recorded. For further details of the experimental setup, see section 2.4.

In this experiment, the standard stimulus was green hue, while two deviant stimuli—blue-green and red—were presented in separate blocks as deviant 1 (blue-green) and deviant 2 (red). The selection of these particular colors was based on their estimated chromatic contrasts relative to the standard stimulus, which were designed to create varying levels of perceptual saliency, thus requiring different degrees of attentional engagement (see section 2.2 for details on stimuli selection). Notably, the chromatic contrasts were expected to evoke

distinct patterns of neural and behavioral responses, particularly between participants with typical trichromacy and those with deuteranopia, where the perceptual saliency of deviant stimuli would theoretically reverse.

The experimental design aimed to exploit these differences in chromatic perception across different color vision phenotypes, allowing for investigation of both individual variation in color processing and its influence on attentional influence. The random presentation order was adjusted to ensure that the ratio of standard to deviant stimuli remained constant across session, which is ten consecutive blocks, thus preventing potential learning effects.

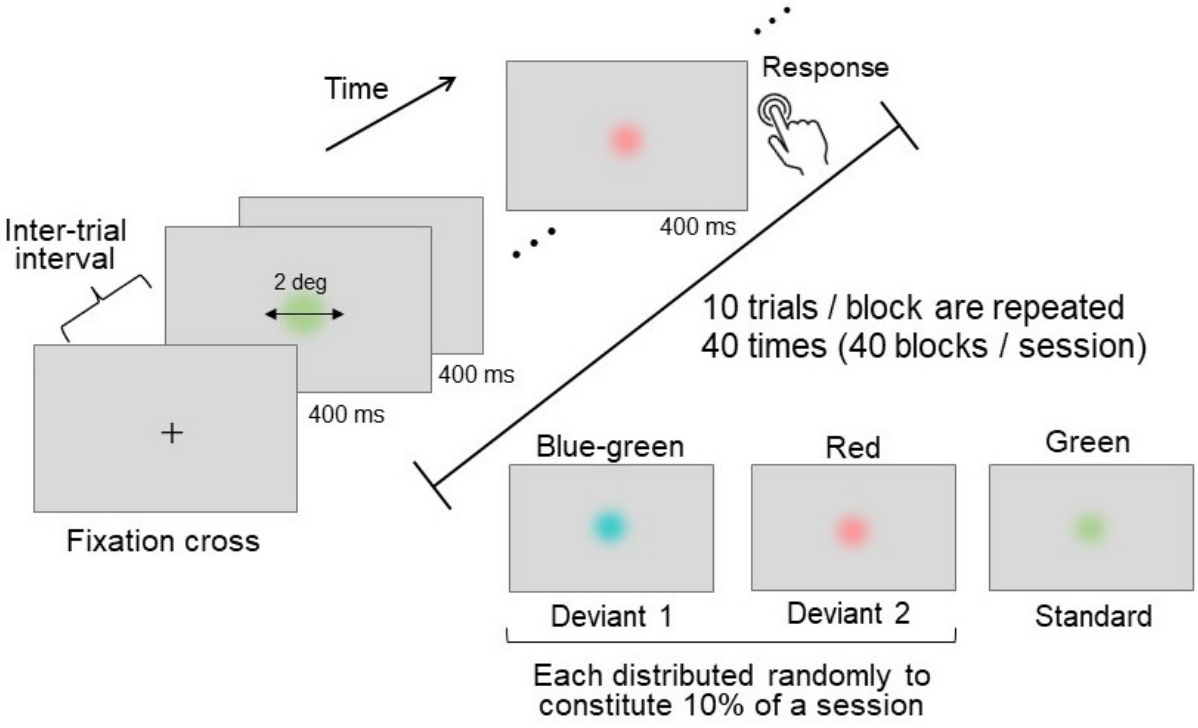

Fig. 2.3 Schematics of the oddball task. Three distinct colors were used: two deviant stimuli (presented rarely) and one standard stimulus (presented frequently). Each stimulus was presented for a duration of 400 ms , with an inter-trial interval of 1,200–1,600 ms. Participants were instructed to press a button immediately upon detecting a deviant stimulus.

2.4 Apparatus

The experimental stimuli were presented on a calibrated 32-inch Full HD LCD monitor (Display++, Cambridge Research Systems Ltd.), linearized to ensure accurate color rendering. Paired with an image processor (Bits#, Cambridge Research Systems Ltd.), the display was capable of presenting colors at a 14-bit resolution with a refresh rate of 120 Hz. The high resolution allowed for precise chromatic and luminance control, which was essential for manipulation of color contrasts in the experiment.

A spectroradiometer (SR-LEDW-5N, Topcon Technohouse) was used prior to the experiment, ensuring that the colors matched their intended coordinates in the CIE 1976 u', v' uniform chromaticity space (see section 2.2 for further details). All experimental procedures were implemented and controlled using a custom program developed in MATLAB (MathWorks Inc.), utilizing the Psychotoolbox-3 extension for accurate visual and timing control (Brainard and Vision, 1997; Kleiner et al., 2007; Pelli and Vision, 1997).

EEG signals were recorded using a 64-channel amplifier (ActiChamp Plus, Brain Products GmbH), with active electrodes placed according to the modified international 10-20 system (Oostenveld and Praamstra, 2001). An electrode cap (actiCap slim, Brain Product GmbH), of either 56 or 58 cm head circumference, was fitted to each participant. To improve contact and minimize noise, electrode gel (V16 SuperVisc High-Viscosity Gel, NEUROSPEC AG) was applied between electrodes and scalp surface. Impedance was measured for each electrode to ensure it was below 10 $k\Omega$ before recording. The signals were digitized and processed at a 1,000 Hz sampling rate to capture neural responses with high temporal resolution.

Precise synchronization between the stimulus presentation, EEG data collection, and behavioral responses was critical for the oddball task. A trigger box, connected via a parallel port to the EEG amplifier, recorded both the onset of stimuli and participants' button press

responses. Additionally, small photoelectric sensors (MaP1180PS2A, NIHON SANTEKU Co., Ltd) were positioned at the edges of the monitor, detecting binary luminance modulations in real-time during the task, ensuring the exact timing of stimulus presentation could be captured and logged for each trial. Participants' responses were recorded via a manual button press, linked directly to the trigger box.

2.5 Procedure

Participants were seated 57 cm from the display in a dark, windowless room with the lights turned off to eliminate external light. They were given time to adjust to the darkness during the instruction and practice sessions. Each participant wore an electrode cap, and their gaze was directed at the screen's center.

2.5.1 Flicker Photometry

Before the oddball task, the luminance of the stimuli (blue-green, red, and green) was equalized to 20 cd/m^2 (D65) using flicker photometry. In this process, participants identified the point at which flickering between the stimulus and the D65 background, alternating at 15 Hz, was no longer perceivable, indicating equiluminance. Participants adjusted the stimulus luminance with arrow keys (0.1 cd/m^2 per press), combining the up-down method with the method of limits to fine-tune the adjustment until the flicker disappeared.

The equiluminance adjustment was repeated six times for each stimulus (blue-green, red, and green), starting from either 23 cd/m^2 or 17 cd/m^2. The averaged luminance values for

each stimulus were then applied individually to the corresponding stimuli during the main oddball experiment.

Details of the instructions given to participants are presented in Appendix F. For further information on flicker photometry as a luminance equality measurement method and its physiological background, see section 1.8.

2.5.2 Main Task

In each trial, a disk-shaped stimulus was presented at the center of the screen for 400 ms, with random inter-trial intervals between 1,200 – 1,600 ms. The stimuli had a visual angle of 2° with edges blended into the neutral gray (D65) background. Standard and deviant stimuli followed an 8:2 ratio (Luck, 2014; Potts, 2004), with equal representation of the two deviant stimuli (blue-green and red). Ten trials formed a block, and 40 blocks were presented per session, with breaks between blocks. Only one type of deviant stimulus appeared per block to avoid confusion, and some blocks contained more than one deviant stimulus. For detail of the intentions behind the task design, see section 1.6 for more information.

Instructions did not use color names; instead, participants were shown stimulus sequences. After completing three practice blocks, participants were asked if they understood the task. Additional practice was provided if necessary.

Each session consisted of 40 blocks, repeated twice with a 10-minute break, for a total of 800 trials (640 standard, 80 deviant 1, and 80 deviant 2 trials). Participants responded by pressing a button as quickly as possible upon detecting a deviant stimulus. The monitor was turned on at least 30 minutes before the experiment to ensure consistent output.

The details of the instruction given for participants are presented in Appendix F.

2.6 Behavioral Analysis

Reaction times (RTs) were analyzed using linear mixed-effects (LME) models (Harrison et al., 2018) to examine the effects of chromatic sensitivity variations, stimulus conditions, and their interactions while accounting for individual variability. LME models are an extension of simple linear models which allows for inclusion of both fixed and random effects, making them suitable for capturing the influence of participant-specific differences on RTs.

A key objective of this analysis was to examine the effects of individual chromatic sensitivity differences, as measured by red-green thresholds, along with traditional categorical distinctions of color vision types (typical vs. anomalous trichromats). By incorporating continuous chromatic sensitivity variations in the red-green threshold model, it was aimed to assess how these continuous variations might impact RTs, offering a more nuanced understanding compared to the conventional categorical approach.

The analysis proceeded with the comparisons of these LME models. The simple model included only stimulus conditions (deviant 1 or deviant 2) as a fixed effect. The color vision model introduced a categorical variable for color vision type (typical or anomalous trichromats), and the red-green threshold model incorporated continuous variations in chromatic sensitivity (measured by red-green threshold by the CAD test). These models are specified as follows:

- **Simple:** Trial-based RTs $\sim$ Condition + (1 | Participants)
- **Color vision:** Trial-based RTs $\sim$ ColorVision * Condition + (1 | Participants)
- **Red-green threshold:** Trial-based RTs $\sim$ RGthreshold * Condition + (1 | Participants)

Here, *ColorVision* represents the participant's categorical color vision type, while *RGthreshold* represents the red-green threshold, and *Condition* refers to stimulus condition. The inclusion of participants as random intercepts (1 | *Participants*) accounted for random effects related to individual differences.

The model comparisons were conducted using likelihood ratio tests to evaluate whether the addition of color vision type or red-green threshold significantly improved model fit comparatively from the simple model. Standard model fit criteria (AIC , BIC , and log-likelihood) were assessed whether inclusion of color vision type or red-green thresholds improved the model's explanatory power from the baseline simple model.

To assess the validity of the LME model, residual analysis was conducted (Darlington and Hayes, 2016). Residuals, calculated as the difference between the log-transformed RTs (observed values) and the predicted values from the model's fixed and random effects, were examined. A positive residual indicates that the model overestimated RT (i.e., predicted a faster response), while a negative residual indicates underestimation (i.e., predicted a slower response). Residual analysis is essential for ensuring the model assumptions hold, including the independence of errors and unbiased predictions. A violation of constant independence or randomness in the residuals against the prediction would suggest bias in the model's prediction. To diagnose the validity of the model, a histogram of the residuals was inspected to assess normality, which supports the reliability of the model and confirms that the linearity assumption was not violated (Altman and Krzywinski, 2016). Additionally, Cook's distance

(Cook, 1979) was calculated to check for any influential outliers that might disproportionately affect the model's predictions. All data points fell below the threshold (4 / number of data points), indicating the absence of major outliers that could interfere with the model.

To visualize individual performance, mean log-transformed RTs were calculated for each stimulus condition. Although the deuteranopic participant was excluded from group-based analyses due to sample size limitations (n = 1), a paired t-test was conducted using the log-transformed data to assess differences between conditions.

For overall behavioral performance, group mean hit rates were computed for deviant stimuli (1 and 2), and false alarm rates were calculated for standard stimuli. RTs exceeding 900 ms were treated as outliers and excluded from the analysis. All statistical analyses were performed using MATLAB 2023a (MathWorks, Inc.), with the LME models fitted using the fitlme function.

2.7 EEG recording and data analysis

2.7.1 Data Preprocessing

EEG data were recorded with a sampling rate of 1000 Hz and processed using EEGLAB (version 2022.0; Delorme and Makeig 2004) in MATLAB (MathWorks, Inc.). The dataset was organized according to the Brain Imaging Data Structure (BIDS; Gorgolewski et al. 2016) with extensions for EEG data (Pernet et al., 2019). Preprocessing began with bandpass filtering the data between 0.5 Hz and 30 Hz. This bandpass range was chosen to focus on ERPs, which are known to be linked to brain activity engaged in cognitive tasks (Luck, 2014; Picton et al., 1995).

To improve the clarity and quality of the data, two EEGLAB plugins were applied: ICLabel (Pion-Tonachini et al., 2019) and CleanRawdata (Delorme, 2021; Miyakoshi and Makeig, 2022). ICLabel was used to differentiate independent components (IC) associated with brain activity (labeled as Brain) from non-neural sources (labeled as: *Muscle*, *Eye*, *Heart*, *Line Noise*, *Channel Noise*, and *Other*) based on spatiotemporal features of EEG (Zapata-Saldarriaga et al., 2023). Components related to eye movements, muscle activity, or channel noise were rejected if they had a probability of 90% or higher of being a non-brain source. CleanRawdata further refined the data by detecting and removing noisy channels and artifact-laden data segments, such as low-frequency drifts and flatlines, using thresholds based on signal amplitude and variance. These processes followed preprocessing guidelines proposed by Delorme (2023), with interpolation for rejected channels was conducted by estimating data from neighboring electrodes to maintain data integrity.

An epoch of 1,000 ms was extracted for each trial, and baseline correction was applied by subtracting the average activity of the 100 ms pre-stimulus period. This procedure establishes a 0 μV baseline, ensuring that recorded activity is consistently relative to the pre-stimulus period (Keil et al., 2014; Luck, 2014; Murray et al., 2008).

Electrode impedance was monitored throughout the experiment to ensure it remained below 10 $k\Omega$, as higher impedance can introduce noise into the recordings. During inter-block breaks, electrode placement was checked, and any necessary adjustments were made in cases where significant noise was detected.

2.7.2 Data Analysis

The EEG data were segmented into 1,000 ms epochs following stimulus onset. These epochs were averaged for each participant and then grand-averaged across all participants to

generate the event-related potentials (ERPs) for each stimulus condition within the two color vision groups: typical and anomalous trichromats. In addition, 95% confidence intervals (CIs) were calculated to represent variability among participants.

The analysis focused on the P3 component, a late positive deflection typically observed at centroparietal electrodes (Cz, CPz, and Pz) (Potts, 2004; Romero and Polich, 1996), which is closely linked to attentional processing in visual oddball tasks. Although the P3 component can be further divided into subcomponents P3a and P3b (Comerchero and Polich, 1999; Mccarthy et al., 1997), their temporal and spatial overlap often makes them difficult to distinguish in practice. P3a is associated with frontal activity linked to attentional switching, whereas P3b reflects context-updating and memory processes, typically observed at parietal sites (Comerchero and Polich, 1999; Donchin and Coles, 1988; Donchin et al., 1997). Given these challenges and the characteristics of our experimental paradigm, the component is referred to as P3, aligning with prior research in similar contexts (Holmes et al., 2009).

The P3 component, peaking around 400 ms post-stimulus, is elicited by rare or unexpected stimuli and reflects attentional resource allocation (Alho et al., 1992; Polich, 1987; Potts, 2004). Larger P3 amplitudes are associated with stimuli that demand greater perceptual and cognitive effort, reflecting increased allocation of attentional resources (Alho et al., 1992; Grasso et al., 2009; Isreal et al., 1980; Polich, 1987; Potts, 2004). In this study, P3 amplitude was interpreted as an index of neural sensitivity to task difficulty, with chromatic sensitivity expected to influence the level of challenge for each group. Specifically, deviant 1 (blue-green) was hypothesized to be more challenging for typical trichromats, whereas deviant 2 (red) was expected to pose greater challenges for anomalous trichromats.

To evaluate the relationship between stimulus conditions and P3 amplitude, linear mixed-effects (LME) models were employed, as in the RT analysis. This model choice allowed us to examine whether neural sensitivity to chromatic variation diverged from or remained consistent with behavioral responses. A simple model, which did not account for chromatic

sensitivity differences, was compared to models that included color vision type or red-green threshold as predictors of P3 amplitude. These models were formulated as follows:

- **Simple:** P3 $\sim$ Condition + (1 | Participants)
- **Color vision:** P3 $\sim$ ColorVision * Condition + (1 | Participants)
- **Red-green threshold:** P3 $\sim$ RGthreshold * Condition + (1 | Participants)

P3 amplitude (*P3*) was defined as the maximum positive activity occurring between 301 ms and 600 ms (Glazer et al., 2018), derived from averaged signals at Cz, CPz, and Pz. In these models, *P3* served as the dependent variable, with *Condition* representing the stimulus type (deviant 1 or deviant 2) and *ColorVision* or *RGthreshold* representing chromatic sensitivity as fixed effects. *Participants* were treated as a random effect to account for inter-individual variability.

Residual analysis was performed to validate the LME model for P3 amplitude data. Residuals, calculated as the difference between observed P3 amplitudes and the model's predicted values, were inspected to ensure the model's assumptions were met. A histogram of residuals was examined to check for normal distribution, confirming the reliability of the model's predictions.

In addition, Cook's distance was calculated to identify any influential outliers that could disproportionately impact the model. All data points were below the threshold (4/number of data points), indicating no significant outliers were present to interfere with the model's predictions.

ERPs at frontal (AF3, AFz, AF4) and occipital (PO7, O1, O2, and PO8) electrodes are visually inspected to verify the spatiotemporal evolution of neural responses across scalp regions.

To further investigate the spatiotemporal dynamics of neural activity, a cluster-based permutation test was applied. This nonparametric, data-driven approach evaluates statistical differences across time points and electrode locations without the need for predefined assumptions, while controlling for Type I error rates (Maris and Oostenveld, 2007; Sassenhagen and Draschkow, 2019). The permutation test assessed whether neural responses from different stimulus conditions or color vision groups were sampled from the same distribution.

The cluster-based permutation test compared i) stimulus color conditions within each color vision type and ii) color vision groups under the same stimulus conditions. This analysis was conducted using the FieldTrip toolbox (Oostenveld et al., 2011). The mean ERPs from 64 electrodes during the 600 ms following stimulus onset were analyzed to capture both perceptual and cognitive processes, including the P3 component.

The time window was selected based on prior evidence that the P3 component typically occurs between 300 ms and 600 ms after stimulus onset (Glazer et al., 2018; Romero and Polich, 1996). Importantly, limiting the time window enhances the sensitivity of the cluster-based permutation test, as extending the analysis over longer intervals can dilute the statistical power of detecting localized effects (Oostenveld et al., 2011).

Clusters were formed when neighboring electrodes or consecutive time points exhibited statistically significant t-values ($p < 0.05$). The size of a cluster was defined as the sum of t-values across the spatial and temporal dimensions. Positive or negative clusters were determined based on the sign of the sum of t-values. A Monte Carlo simulation (10,000 iterations) was used to generate a null distribution, and cluster significance was set by

comparing observed cluster sizes against the 2.5% critical value (Bonferroni corrected to 0.625% for four comparisons). Clusters exceeding this threshold were considered significant.

Chapter 3

Results

3.1 Flicker Photometry

Prior to the oddball task, the luminance of the stimuli was individually adjusted to match the gray background using flicker photometry. The average luminance values for deviant 1 (blue-green), deviant 2 (red), and the standard stimulus (green) were 20.49 $\pm$ 0.36, 19.74 $\pm$ 0.37, and 20.11 $\pm$ 0.12 cd/m^2 for typical trichromats (n = 13), respectively; 21.27 $\pm$ 0.086, 18.96 $\pm$ 0.12, and 20.60 $\pm$ 0.095 cd/m^2 for anomalous trichromats (n = 5); and 21.43 $\pm$ 0.30, 19.04 $\pm$ 0.32, and 20.77 $\pm$ 0.58 cd/m^2 for the deuteranope (n = 1) (Table 3.1).

Independent *t*-tests revealed statistically significant differences between color vision types (typical and anomalous trichromats) for each stimulus condition: deviant 1 ($t(16)$ = -4.68, p = 0.0003, Cohen's d = 2.35), deviant 2 ($t(16)$ = 4.55, p = 0.0003, Cohen's d = 2.30), and the standard stimulus ($t(16)$ = -2.50, p = 0.024, Cohen's d = 1.25) (Figure 3.1).

The luminance levels identified for each participant are presented in Appendix A for further details.

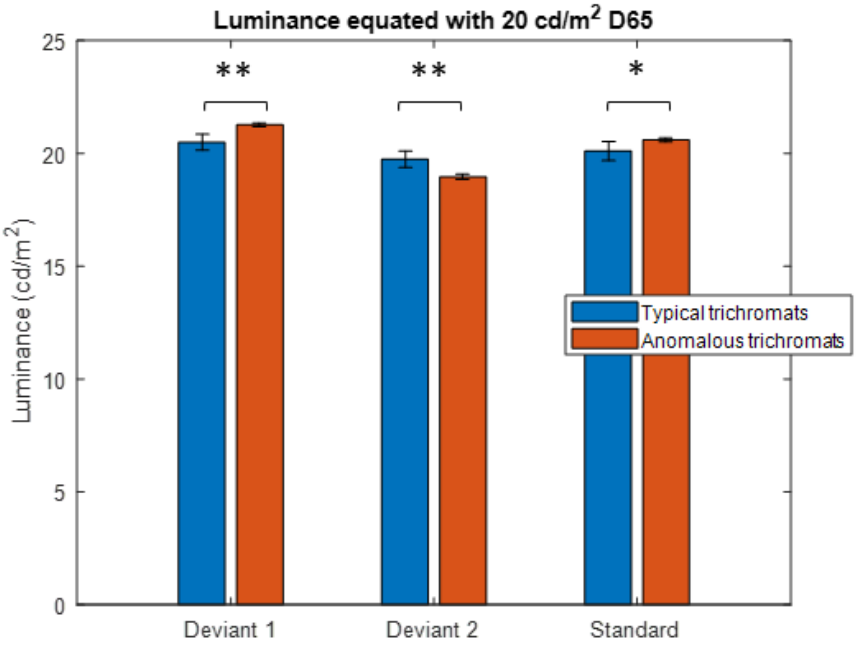

Fig. 3.1 Comparison of stimulus luminance adjusted to match $20 cd/m^2$ D65 between color vision groups (typical trichromats: n = 13, anomalous trichromats: n = 5), using the flicker photometry method. Error bars indicate the standard deviation. Significant differences are marked with ** ($p < 0.0005$) and * ($p = 0.05$).

Color vision type	Mean luminance ± Standard deviantion (cd/m^2)		
	Deviant 1	Deviant 2	Standard
Typical trichromats	20.49 ± 0.36	19.74 ± 0.37	20.11 ± 0.43
Deteranomalous trichromats	21.27 ± 0.09	18.96 ± 0.12	20.60 ± 0.10
Deuteranope	21.43 ± 0.30	19.04 ± 0.32	20.78 ± 0.58

Table 3.1 Mean stimulus luminance adjusted to match an equivalent of 20 cd/m^2 D65 for each color vision type, as measured using the flicker photometry method. Actual luminance used in the experiment was determined based on each participant's individual adjustment rather than group-averaged values (see appendix A for the details). Note that the deuteranopia result represents the mean for a single participant due to limited sample size. The stimulus colors are identified as blue-green for deviant 1, red for deviant 2, and green for the standard condition.

3.2 Behavioral Result

3.2.1 Behavioral Performance

Several reaction time (RT) records were identified as outliers and excluded from the analysis. For typical trichromats, one RT from deviant 1 (919 ms) and two from deviant 2 (1,588 and 1,069 ms) were identified as outliers values, all belonging to the same participant. Similarly, anomalous trichromats showed three outliers: one RT from deviant 1 (986 ms) and two from deviant 2 (1,051 and 981 ms), all from a single participant.

Hit rates, representing correct responses to target stimuli, were consistently high across all color vision groups. Typical trichromats achieved hit rates of 99.71% for deviant 1 and 99.42% for deviant 2. Anomalous trichromats reached 100% and 99.50%, respectively,

while the deuteranope participant achieved a hit rate of 100% for both deviants. False alarm rates, reflecting incorrect responses to the non-target standard stimulus, were notably low. Typical trichromats had a false alarm rate of 0.1%, anomalous trichromats had 0.05%, and the deuteranope participant had 0.17%. Due to the small number of false alarms and the experiment design, it was not possible to determine which deviant stimuli were more prone to false detection.

Figure 3.2 presents the log-transformed individual mean RTs in separate plots for typical trichromats and for anomalous trichromats along with the deuteranope participant.

The deuteranope participant demonstrated significantly faster RTs to deviant 2 (red) (2.57 $\pm$ 0.06) compared to deviant 1 (blue-green) (2.59 $\pm$ 0.06), indicating a quicker response to the stimulus predicted to be less salient for them ($t(158) = 2.18$, $p = 0.03$, Cohen's $d = 0.34$). This result was unexpected, as based on the participant's color vision type and measured red-green sensitivity, red was predicted to be less salient than blue-green.

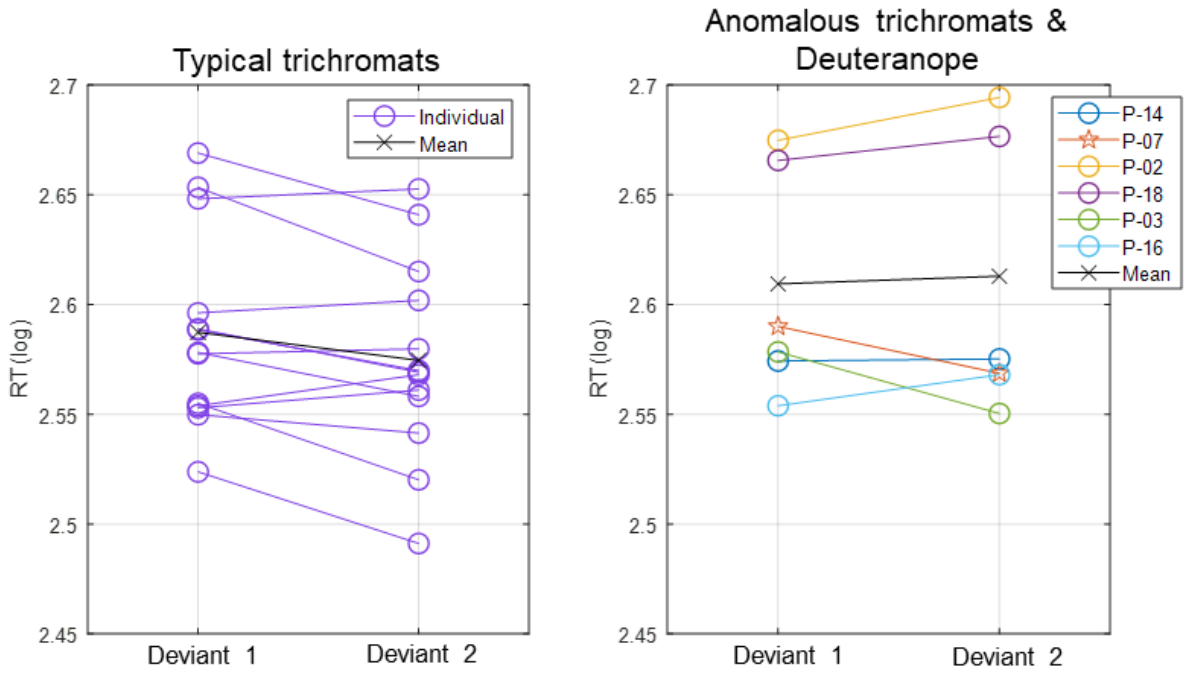

Fig. 3.2 Individual mean reaction times (RTs) for each participant, along with group mean RTs for typical trichromats (n = 13) and anomalous trichromats (n = 5) for deviant stimuli 1 (blue-green) and 2 (red). For anomalous trichromats, symbol colors correspond to the participant identifiers in Table 1, listed in descending order by red-green threshold (where a larger red-green threshold indicates reduced red-green sensitivity) and matching the order in the legend of the right panel. Stars represent the deuteranope's individual mean RTs (n = 1), while circles indicate individual mean RTs for typical and anomalous trichromats.

3.2.2 Comparative Analysis with LME Models

The impact of chromatic sensitivity on behavioral performance was evaluated using a likelihood ratio test, alongside model fit indices such as AIC, BIC, and Log-Likelihood values from the mixed linear effect (LME) models. A comparison was made between a simple model, which included only stimulus condition as a fixed effect, and two more complex

models: the color vision type model (which included color vision type as an additional fixed effect) and the red-green threshold model (which incorporated red-green threshold as a fixed effect). Both of the complex models showed a significantly better fit compared to the simple model, suggesting that chromatic sensitivity is a crucial factor in predicting behavioral performance. Specifically, the color vision type model resulted in a significant improvement over the simple model ($p = 0.007$), while the red-green threshold model provided a slightly superior fit compared to the color vision type model ($p = 0.006$), as summarized in Table 3.2.

This marginal improvement in fit for the red-green threshold model was further evidenced by slightly better AIC, BIC, and Log-Likelihood values: the red-green threshold model had an AIC of −7,218.415, BIC of −7,182.676, and Log-Likelihood of 3,615.207, while the color vision type model had an AIC of −7,218.213, BIC of −7,182.474, and Log-Likelihood of 3,615.107 (see Table 3.2). Despite the models having comparable statistics, the red-green threshold model provided a marginally more precise estimate of behavioral performance, potentially due to its finer representation of chromatic sensitivity variation.

Within the red-green threshold model, a significant interaction was observed between red-green threshold and stimulus condition ($p = 0.008$), along with a significant main effect for stimulus condition ($p = 0.001$) (see Table 3.3). The interaction indicates that as the red-green threshold increased (reflecting lower chromatic sensitivity), the difference in reaction times (RTs) between deviant 1 and deviant 2 became smaller. The main effect of -0.008 suggests that, at an average red-green threshold level (standardized as zero after z-scoring), RTs were generally faster for deviant 2 than for deviant 1.

To further validate the significance of the interaction between red-green threshold and stimulus condition, a likelihood ratio test was performed comparing the interaction model with a model excluding the interaction term. The test showed a significant improvement in fit for the interaction model ($p = 0.008$), as indicated by a lower AIC (interaction model: −7,218.415, without interaction model: −7,213.323) and higher Log-Likelihood (interaction

model: 3,615.208, without interaction model: 3,611.661) (see Table 3.4). This suggests that the interaction term enhances the model's ability to predict behavioral performance across varying levels of chromatic sensitivity.

As shown in Figure 3.3, Residuals from the red-green threshold model were examined to ensure the assumptions of the LME models were met. A histogram of residuals showed a normal distribution, confirming the reliability of the model predictions and indicating no significant bias. Additionally, Cook's distance was calculated, and all values fell below the threshold, indicating no major outliers that could disproportionately affect the model's predictions.

1. Simple: Trial-based RTs $\sim$ Condition + (1 | Participants)
2. Color vision: Trial-based RTs $\sim$ ColorVision * Condition + (1 | Participants)
3. RG threshold: Trial-based RTs $\sim$ RGthreshold * Condition + (1 | Participants)

Model	**DF**	**AIC**	**BIC**	**Log-Likelihood**	**LRStat**	**deltaDF**	***p*-value**
Model 1	4	−7,212.238	−7,188.412	3,610.119			
Model 1 vs 2	6	−7,218.213	−7,182.474	3,615.107	9.976	2	0.007*
Model 1 vs 3	6	−7,218.415	−7,182.676	3,615.207	10.177	2	0.006*

Table 3.2 Results of the likelihood ratio tests comparing the simple LME model on reaction times (RTs) with two more complex models: Model 2, which includes categorical color vision type as a fixed effect, and Model 3, which includes continuous red-green threshold as a fixed effect. A single asterisk (*) indicates $p < 0.05$.

LME model	Trial-based RTs ∼ RGthreshold * Condition + (1 | Participants)						
Fixed Effect	**Estimate**	**SE**	**tStat**	**DF**	***p*-value**	**95% CI Lower**	**95% CI Upper**
Red-green threshold	0.016	0.010	1.501	2,850	0.133	-0.005	0.036
Stimulus Condition	-0.008	0.003	-3.276	2,850	0.001*	-0.013	-0.003
Red-green threshold: Stimulus Condition	0.007	0.003	2.665	2,850	0.008*	0.002	0.012

Table 3.3 Summary of trial-based reaction times (RTs) analyzed using an LME model with red-green threshold added as a fixed effect. This model demonstrated a better fit to the data compared to the model including only color vision type. A significant interaction was found between color vision type and stimulus condition. A single asterisk (*) indicates $p < 0.05$.

1. Without interaction: Trial-based RTs ∼ Condition + RGthreshold + (1 | Participants)
2. With interaction: Trial-based RTs ∼ Condition * RGthreshold + (1 | Participants)

Model	**DF**	**AIC**	**BIC**	**Log-Likelihood**	**LRStat**	**deltaDF**	***p*-value**
Model 1	5	-7213.323	-7183.540	3611.661			
Model 2	6	-7218.415	-7182.676	3615.208	7.092	1	0.008*

Table 3.4 Results of the likelihood ratio test assessing the effect of an interaction term in the LME model on reaction times (RTs), with the model incorporating the red-green threshold. A single asterisk (*) indicates $p < 0.05$.

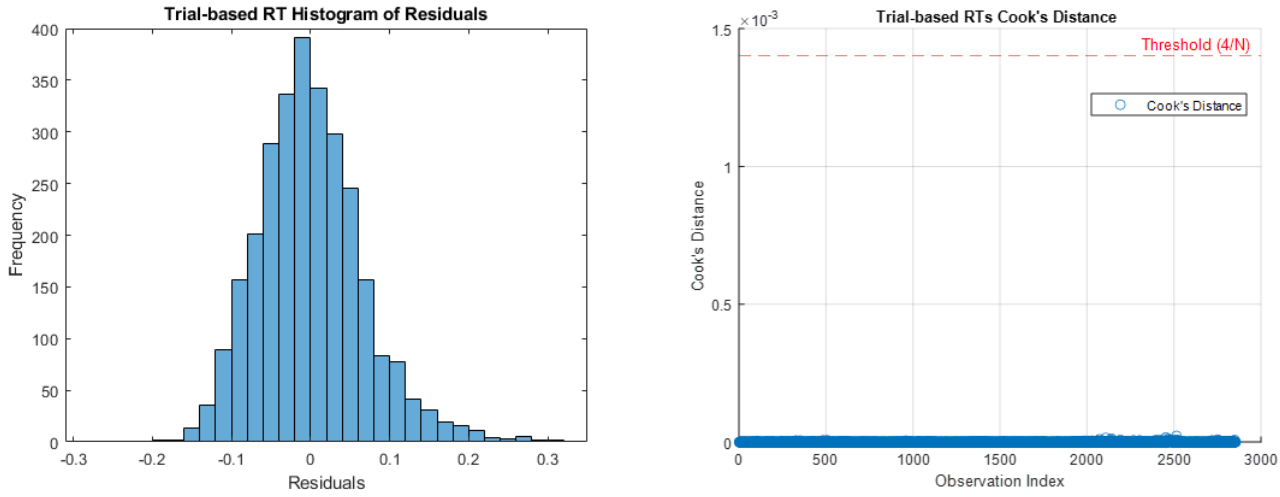

Fig. 3.3 Residual analysis for the red-green threshold model in the trial-based RT LME model. The histogram of residuals (left) shows a normal distribution, supporting the validity of the model assumptions. Cook's distance (right) indicates that all data points fall below the threshold, suggesting no significant outliers that could influence the model.

3.3 Electrophysiological Results

3.3.1 ERPs and LME Model Analysis

Figure 3.4 illustrates the ERPs for each color vision group across three distinct scalp regions. The central column highlights the ERPs in the parietal region, averaged across electrodes Cz, CPz, and Pz. In both color vision groups, the P3 component was clearly visible in response to the deviant stimuli, while the response to the standard condition was notably suppressed. Notably, the 95% confidence intervals for anomalous trichromats (n = 5) were wider than those for typical trichromats (n = 13), reflecting greater variability in the former group's neural responses.

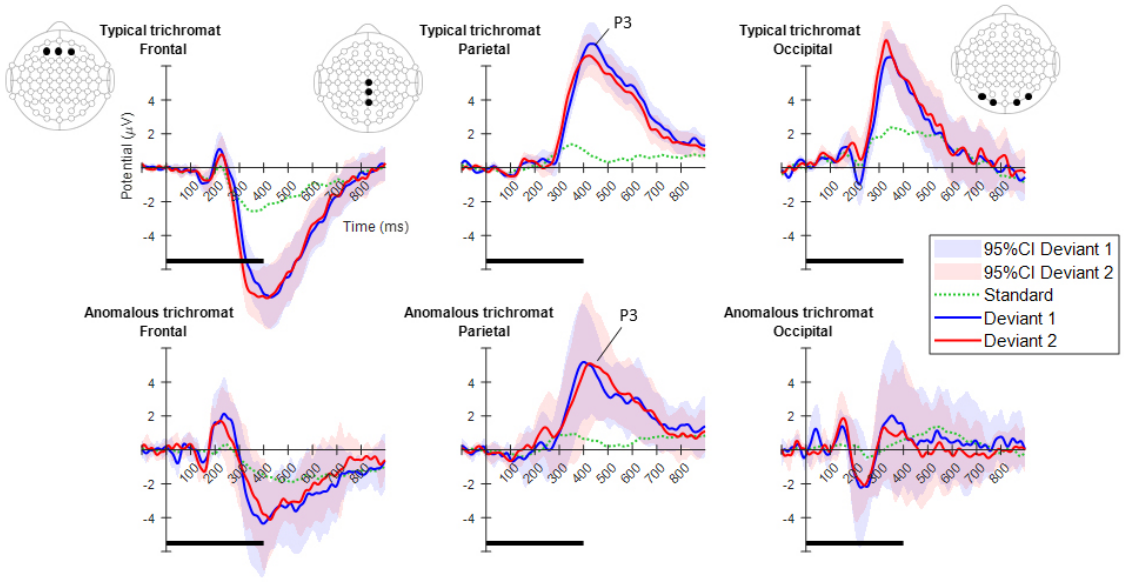

Fig. 3.4 Mean ERPs for each color vision type across three scalp regions: frontal, parietal, and occipital. From left to right, the plots display ERPs for each region, with corresponding electrode positions marked as black dots on the electrode layout. The top row represents typical trichromats (n = 13), while the bottom row shows anomalous trichromats (n = 5). In each plot, blue and red lines indicate the mean ERPs across participants for deviants 1 (blue-green) and 2 (red), respectively, with shaded areas showing 95% confidence intervals (CIs). A dotted green line represents the mean potential for the standard stimulus, and horizontal black lines at the bottom of each plot denote stimulus duration.

A comparative analysis of LME models revealed that the addition of chromatic sensitivity, whether as a categorical (color vision type) or continuous (red-green threshold) predictor variable, did not significantly improve the model fit compared to the simple model (simple model vs. color vision type model: $p = 0.067$; simple model vs. red-green threshold model: $p = 0.081$). Although neither model reached statistical significance, the color vision type model provided the best overall fit, as indicated by lower AIC, BIC, and Log-Likelihood values. However, this model did not show any significant main effects or interactions, suggesting limited influence of chromatic sensitivity on P3 amplitude (see Table 3.5).

Figure 3.5 presents the individual mean P3 amplitude for each stimulus condition across the color vision groups.

Although either the color vision model nor red-green threshold model contributed significantly to explaining the P3 amplitude, validity of the models were assessed through residual analysis. A histogram of the residuals suggested an approximately normal distribution, though the small sample size made it difficult to clearly discern the shape of the histogram. This analysis confirmed that the model assumptions were not violated. This supports the reliability of the model's predictions, despite the lack of significant findings (see Figure 3.6 left column).

Additionally, Cook's distance was calculated to identify any influence of outliers. While some data points were scattered above zero, all remained well below the threshold, indicating no major outliers that could have disproportionately impacted the model see Figure 3.6 right column.

1. Simple: P3 $\sim$ Condition + (1 | Participants)
2. Color vision: P3 $\sim$ ColorVision * Condition + (1 | Participants)
3. Red-green threshold: P3 $\sim$ RGthreshold * Condition + (1 | Participants)

Model	**DF**	**AIC**	**BIC**	**Log-Likelihood**	**LRStat**	**deltaDF**	***p*-value**
Model 1	4	145.540	151.874	-68.77			
Model 1 vs 2	6	144.125	153.627	-66.063	5.415	2	0.067
Model 1 vs 3	6	144.510	154.012	-66.255	5.030	2	0.081

Table 3.5 Results of likelihood ratio tests comparing a simple LME model (Model 1) for P3 amplitude against two more complex models: Model 2, which includes categorical color vision type as a fixed effect, and Model 3, which includes continuous red-green threshold as a fixed effect.

LME Model: P3 $\sim$ ColorVision * Condition + (1 | Participants)

Fixed Effect	**Estimate**	**SE**	**tStat**	**DF**	***p*-value**	**95% CI Lower**	**95% CI Upper**
Color vision type	2.286	1.364	1.676	32	0.103	-0.492	5.064
Stimulus condition	0.281	0.403	0.697	32	0.491	-0.540	1.101
Color vision type: Stimuli condition	-0.960	0.474	-2.024	32	0.051	-1.925	0.006

Table 3.6 Summary of LME model on P3 amplitude with color vision type included as a fixed effect. The model incorporating color vision type provided a better fit than the model with red-green threshold; however, neither the color vision type model nor the red-green threshold model showed a significant improvement over the simple model.

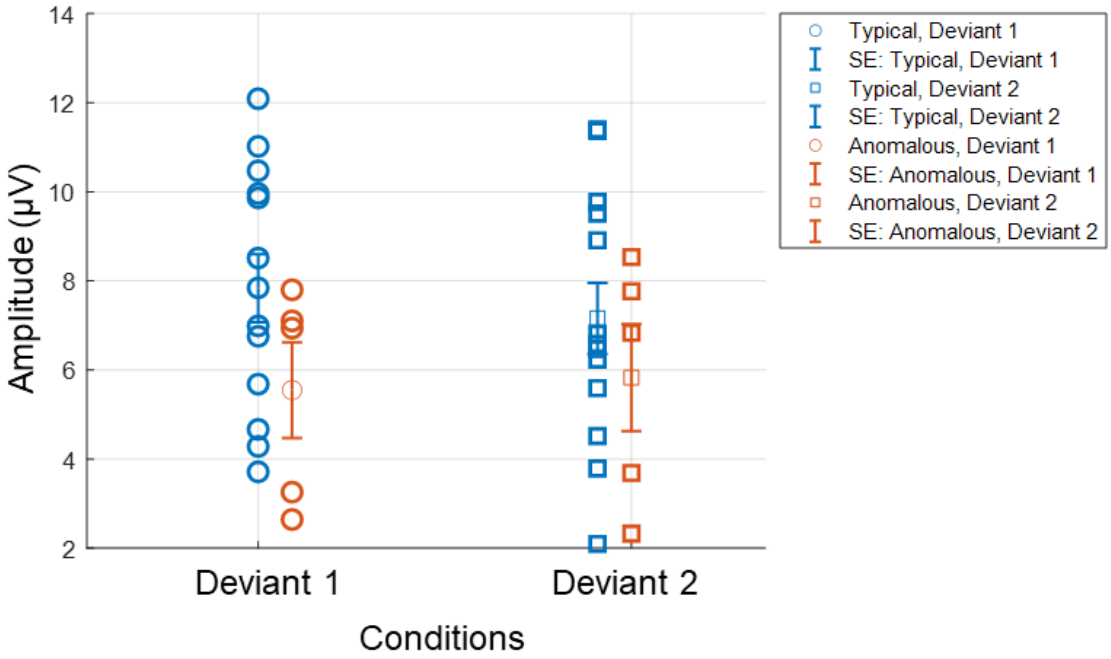

Fig. 3.5 Individual P3 amplitudes across stimulus conditions and color vision types (typical trichromats: n = 13, anomalous trichromats: n = 5). P3 amplitude was computed as the maximum positive activity within the 301–500 ms window, averaged across centroparietal electrodes (Cz, CPz, and Pz). Deviant 1 and Deviant 2 correspond to the stimulus conditions of blue-green and red, respectively. Error bars represent standard error (SE).

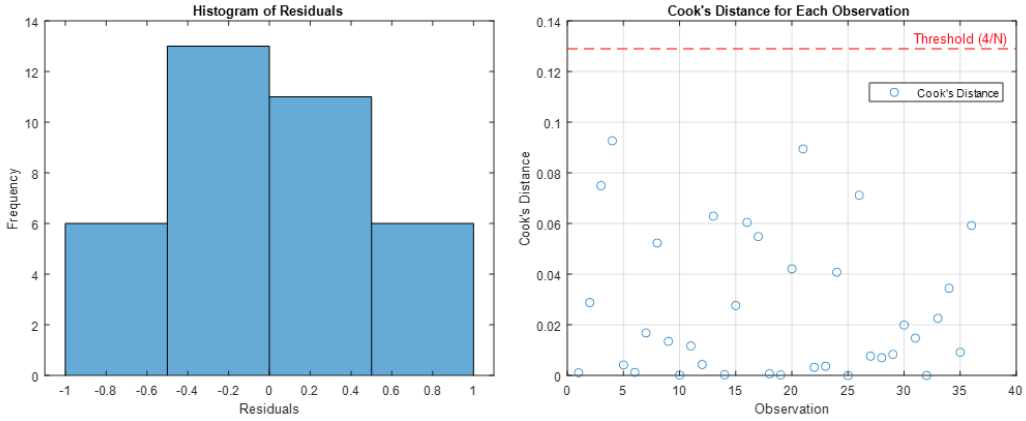

(a) The color vision type model

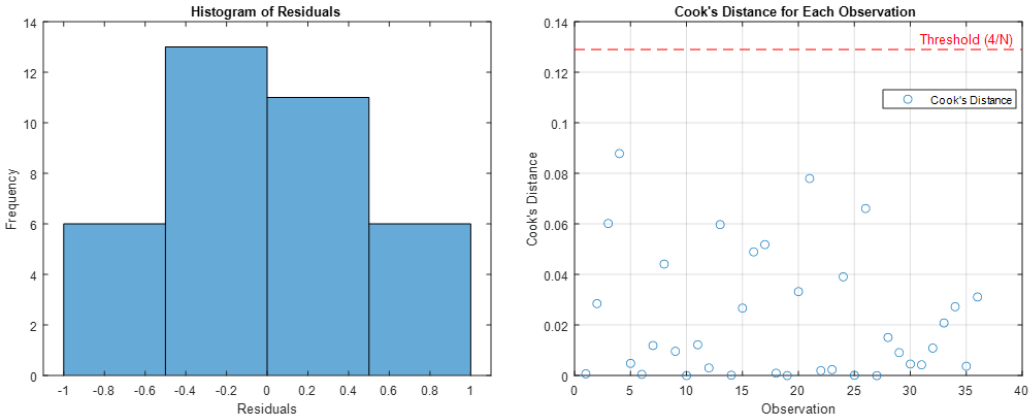

(b) The red-green threshold type model

Fig. 3.6 Residual analysis for P3 amplitude LME models for both (a) the color vision model (top row) and (b) the red-green model (bottom row). The histogram of residuals (left column) shows a normal distribution, supporting the validity of the model assumptions. Cook's distance (right column) indicates that all data points fall below the threshold, suggesting no significant outliers that could influence the model.

3.3.2 Exploratory Analysis of ERPs

The cluster-based permutation analysis identified a significant difference between the two deviant conditions (blue-green and red) in typical trichromats (n = 13) (Figure 3.7). The largest negative cluster exceeded the adjusted threshold (p_{adj} = 0.003), while the largest positive cluster was slightly below the adjusted threshold (p_{adj} = 0.035) (Figure 3.7a). The negative cluster, mapped on scalp topographies, showed that the amplitude for deviant 2 (red) was higher than that for deviant 1 (blue-green), extending from around 200 ms to 350 ms post-stimulus. This cluster was initially localized in the occipital region up to about 240 ms, then gradually expanded toward the parietal area, with the largest amplitude difference observed at approximately 300 ms (Figure 3.8a).

Further comparisons of each deviant stimulus (blue-green and red) with the standard (green) revealed significant differences in typical trichromats (Figure 3.7b, c for temporal distribution and cluster size; Figure 3.8b, c for scalp topographies). For the deviant 1 (blue-green) versus standard (green) comparison, the largest positive cluster, indicating a higher amplitude for deviant 1, was concentrated around occipital and parietal areas (p_{adj} = 0.0004), while the largest negative cluster, indicating a lower amplitude for deviant 1, emerged in frontal regions (p_{adj} = 0.0008). Similarly, when comparing deviant 2 (red) with the standard stimulus, significant positive and negative clusters were observed (positive cluster: p_{adj} = 0.0004; negative cluster: p_{adj} = 0.004), starting around 250 ms post-stimulus and lasting until the end of the analysis window.

In anomalous trichromats (n = 5), no significant differences between the deviant conditions (blue-green and red) were found, as none of the clusters exceeded the adjusted thresholds (positive cluster: p_{adj} = 0.12; negative cluster: p_{adj}= 0.88) (Figure 3.9a). However, significant differences emerged when comparing deviant 1 (blue-green) with the standard (green) stimulus (Figure 3.9b). A positive cluster, indicating a higher amplitude for deviant 1, was

observed in the occipital and parietal regions approximately 350 ms post-stimulus, persisting through the remainder of the analysis window (positive cluster: $p_{adj} = 0.0004$; negative cluster: $p_{adj} = 0.13$) (Figure 3.10a). A similar pattern was found when comparing deviant 2 (red) with the standard (green) stimulus (Figure 3.9c), with a positive cluster appearing in the occipital and parietal regions from 400 to 500 ms post-stimulus (positive cluster: $p_{adj} = 0.0004$; negative cluster: $p_{adj} = 0.12$) (Figure 3.10b).

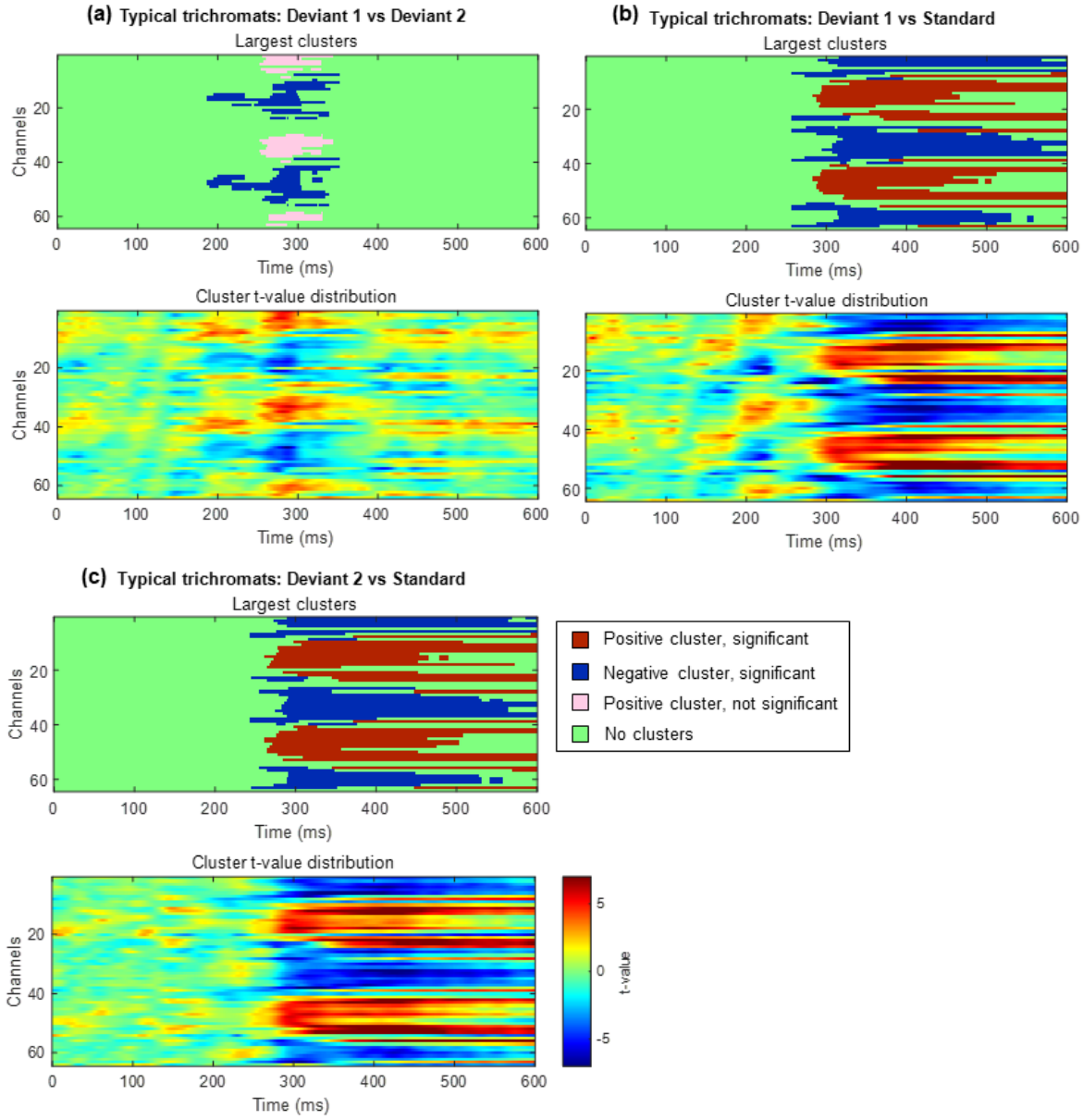

Fig. 3.7 Results of the cluster-based permutation analysis for typical trichromats (n = 13) showing cluster distributions as a function of time and space. Each panel, (a) to (c), consists of two sub-figures. The top sub-figure shows positive and negative clusters that showed the largest absolute cluster size in each sign. Colors of clusters indicate significance of the cluster size. The bottom sub-figure shows topographical image of *t*-value distribution. (a) Comparison between deviant 1 (blue-green) and deviant 2 (red) conditions. (b) Comparison between deviant 1 and standard (green) conditions. (c) Comparison between deviant 2 and standard (green) conditions.

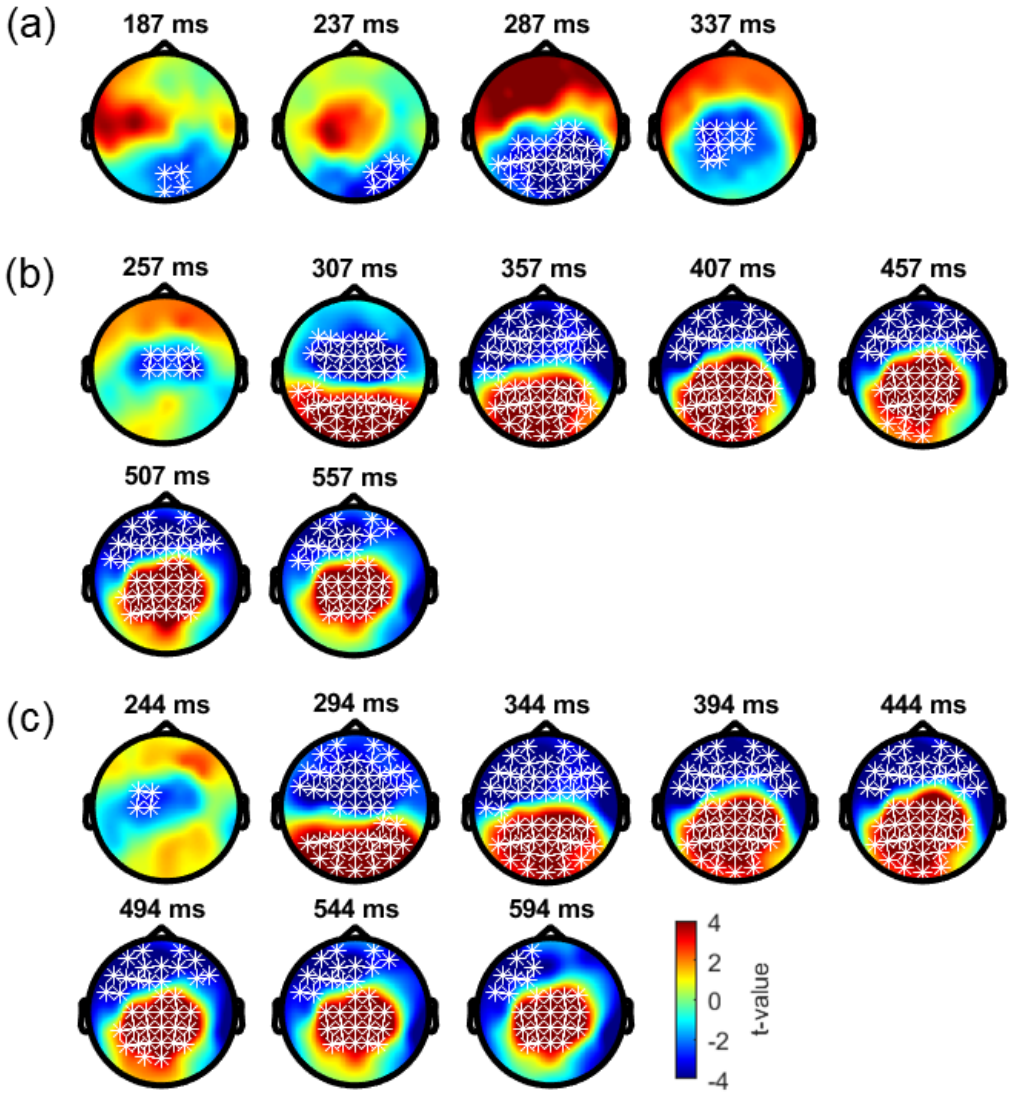

Fig. 3.8 Results of the cluster-based permutation test for typical trichromats ($n = 13$), presented as scalp topographies. (a) Comparison between deviant 1 (blue-green) and deviant 2 (red) conditions. (b) Comparison between deviant 1 and standard (green) conditions. (c) Comparison between deviant 2 and standard conditions. The distribution of t-values is topographically plotted, with electrodes highlighted by white asterisks indicating clusters that exceeded the cluster size threshold. Results are shown in 50 ms intervals within the 600 ms analysis window following stimulus onset.

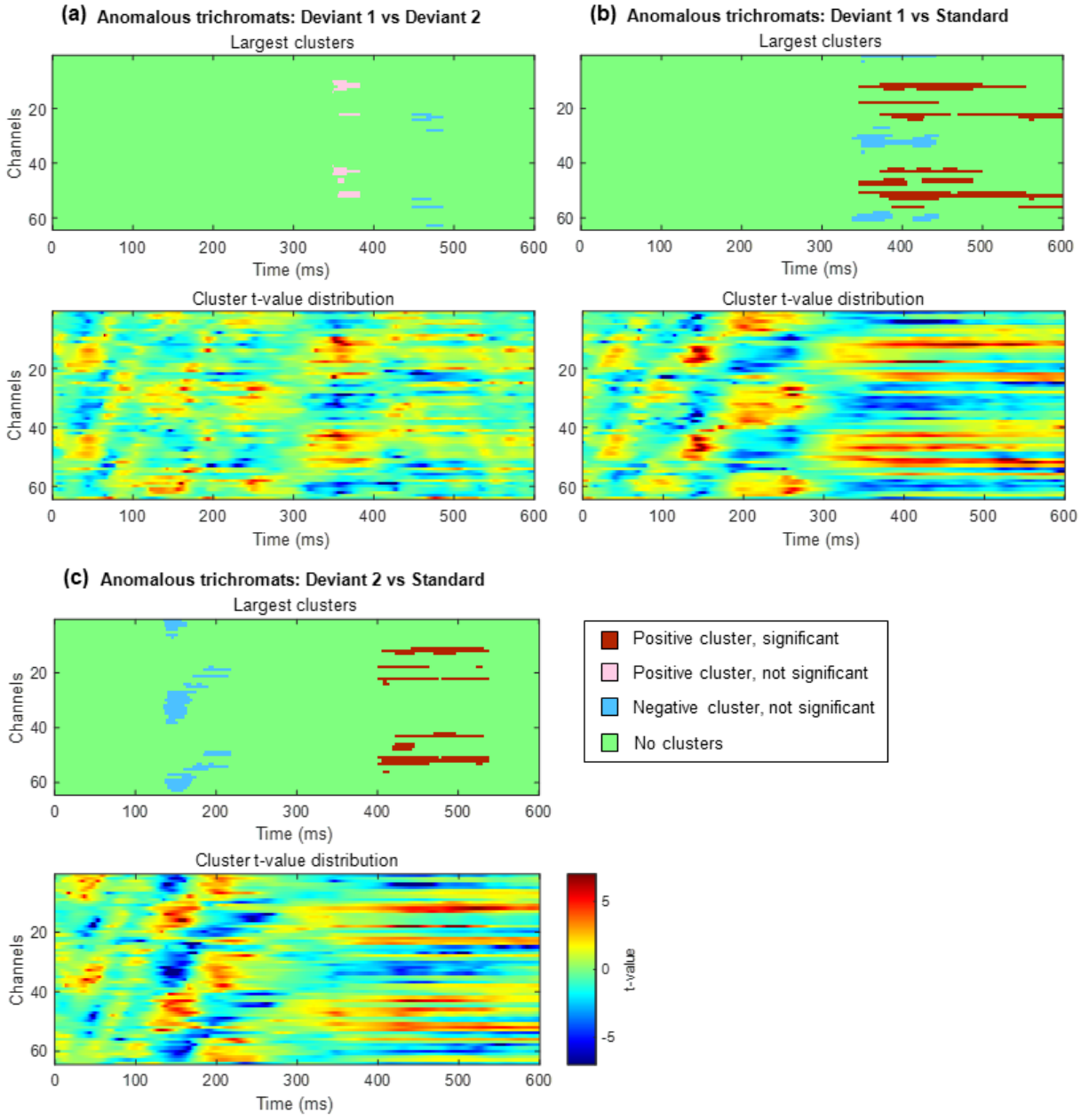

Fig. 3.9 Results of the cluster-based permutation analysis for anomalous trichromats (n = 5) showing cluster distributions as a function of time and space. Each panel, (a) to (c), consists of two sub-figures. The top sub-figure shows largest positive and negative clusters that showed the largest absolute cluster size in each sign. Colors of clusters indicate significance of the cluster size. The bottom sub-figure shows topographical image of *t*-value distribution. (a) Comparison between deviant 1 (blue-green) and deviant 2 (red) conditions. (b) Comparison between deviant 1 and standard (green) conditions. (c) Comparison between deviant 2 and standard (green) conditions.

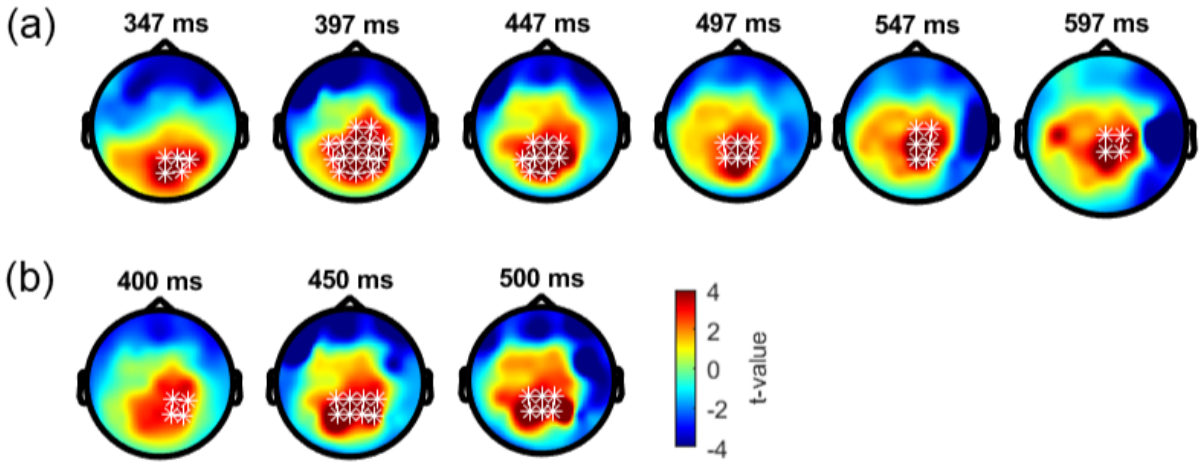

Fig. 3.10 Results of the cluster-based permutation test for anomalous trichromats presented as scalp topography. (a) Comparison between deviant 1 (blue-green) and standard (green) conditions. (b) Comparison between deviant 2 (red) and standard conditions. The distribution of *t*-values are topographically plotted, with electrodes highlighted with white asterisks to indicate locations of the clusters that exceeded the cluster size threshold. Results are shown in 50 ms intervals within the 600 ms analysis window following stimulus onset.

Comparing typical and anomalous trichromats using the cluster-based permutation test did not reveal any significant differences for either deviant condition (deviant 1: positive cluster $p_{adj} = 1$, negative cluster $p_{adj} = 1$; deviant 2: positive cluster $p_{adj} = 0.14$, negative cluster $p_{adj} = 0.66$) (Figure 3.11).

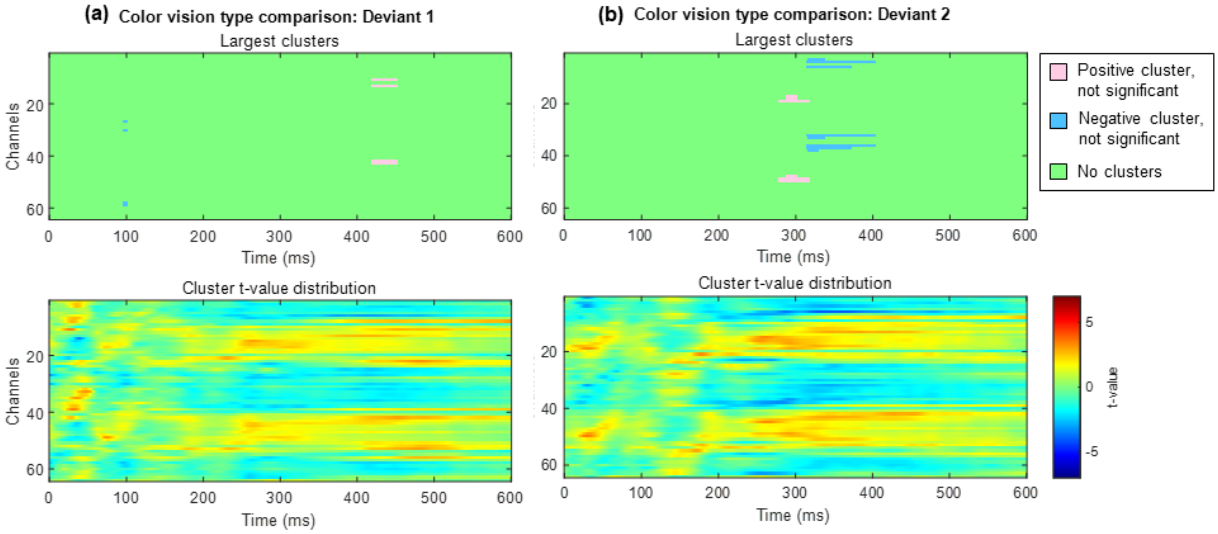

Fig. 3.11 Results of the cluster-based permutation test comparing typical trichromats and anomalous trichromats. Each panel consists of two sub-figures. The top sub-figure shows largest positive and negative clusters that showed the largest absolute cluster size in each sign. Colors of clusters indicate significance of the cluster size. The bottom sub-figure shows topographical image of *t*-value distribution. (a) Comparison of deviant 1 (blue-green). (b) Comparison of deviant 2 (red).

Chapter 4

Discussion and Conclusion

4.1 Restatement of Research Purpose and Aim

The primary purpose of this study was to investigate how neural responses vary or overlap between different color vision types—particularly between typical and anomalous trichromats—during the observation of colors with varying saliency. The focus was on identifying attentional differences that might reflect broader spatiotemporal variations modulated by color saliency. By incorporating both categorical distinctions between color vision types and continuous chromatic sensitivity along red-green axis, it was aimed to provide a more nuanced understanding on how individuals process color. Given existing research highlighting gaps between cone sensitivity and actual discrimination abilities, especially among minority color vision phenotypes, both shared and distinct neural patterns were anticipated, potentially shaped by post-receptoral mechanisms.

4.2 Key Findings

4.2.1 Behavioral Findings

The LME models revealed that continuous chromatic sensitivity (quantified as the red-green threshold) explained the RTs better than the categorical model based on the color vision type. Specifically, a significant interaction between stimulus condition and the red-green threshold highlighted that variations in chromatic sensitivity influenced RT patterns.

The main effect showed that RTs were generally faster for deviant 2 (red) compared to deviant 1 (blue-green), particularly among typical trichromats, the majority group in this study. As this group has a consistent and relatively small red-green threshold (higher discrimination sensitivity), the main effect primarily reflects their RT pattern. This confirms effective stimulus control for these participants.

In contrast, anomalous trichromats demonstrated more variable RT patterns. The interaction term revealed that larger red-green thresholds—indicating reduced chromatic sensitivity—diminished RT differences between the two deviant stimuli. This result contrasts with the expectation of faster RTs to the more salient blue-green deviant for participants with reduced red-green sensitivity.

Individual differences among color vision phenotypes added further complexity. For example, one anomalous trichromat with the largest red-green threshold demonstrated RTs comparable to the fastest typical trichromats. Moreover, a deuteranopic participant demonstrated unexpectedly faster RTs to the red deviant, despite the absence of red-green opponency mechanism according to the color vision test (see Appendix C). This finding is particularly

notable, as it contradicts the expectations based on the participant's color vision profile, instead more closely aligning with the RT patterns observed in typical trichromats.

These suggest that chromatic sensitivity alone does not always predict behavioral performance consistently. For further details on RTs in relation to the red-green threshold, refer to Appendix D.

4.2.2 ERP Findings

P3 amplitude analysis, using LME models, did not reveal significant modulation by either categorical or continuous chromatic sensitivity. However, spatiotemporal analysis using the cluster-based permutation method identified distinct neural patterns in response to saliency difference among typical trichromats. Specifically, the red deviant (more salient for typical trichromats) evoked stronger and faster neural responses, forming a cluster beginning in the occipital region and spreading to the parietal areas, compared to the blue-green stimulus. Additionally, when each was compared to the common green standard, the red deviant showed faster onset than the blue-green stimulus, which supported the experimental design.

In contrast, anomalous trichromats did not show clear saliency-oriented neural clusters when the two deviants were directly compared. However, when the deviants were compared to the standard stimulus, a faster neural response to the blue-green deviant was observed, predominantly in the occipital region to parietal region, with a timing difference approximately 50 ms.

Although the cluster-based analysis does not pinpoint the exact timing or regions (Sassenhagen and Draschkow, 2019), this temporal difference is consistent with previously reported faster behavioral response to blue-green stimulus in visual search task involving anomalous

trichromacy (Sunaga et al., 2013). This provides indirect evidence for saliency-related neural responses in this group, aligning with the expectations and validating stimulus design for saliency modulation.

4.3 Novelty and Contribution

4.3.1 Stimulus Control

One of the strengths of this study was the use of chromatically identical stimuli across participants, regardless of their color vision type or sensitivity variation. This design reflects real-world conditions, where the physical properties of light remain constant across individuals. The exception to this was the adjustment of luminance across all stimuli to match the gray background, ensuring that saliency differences were not confounded by luminance cues.

In anomalous trichromats, individual differences in chromatic sensitivity were a critical consideration, as inconsistent perceived saliency may have impacted both RTs and neural responses. Despite these variations, the cluster-based permutation analysis revealed faster neural responses for the more salient stimulus, validating the overall saliency differences observed in this group. Flicker photometry, used to calibrate luminance, also confirmed that anomalous trichromats exhibited reduced sensitivity to middle-wavelength light, providing further validation for color vision type classification.

4.3.2 Continuous Chromatic Sensitivity

By incorporating variations in continuous chromatic sensitivity, a more nuanced understanding of individual differences in color perception was achieved. The behavioral analysis highlighted the impact of continuous sensitivity variation on RTs, while P3 amplitude was less sensitive to these differences. This suggests that behavioral measures may offer a more reliable indicator of individual differences in chromatic sensitivity, whereas neural measures may require further refinement by considering extra factors or larger samples to detect subtle effects.

4.4 Comparison to the Expectations

4.4.1 Behavioral Results

For typical trichromats, the observed RT patterns aligned well with the expectations, demonstrating faster responses to the more salient red deviant. This reflects their heightened chromatic sensitivity to red-green contrasts. In contrast, anomalous trichromats demonstrated less pronounced RT differences between deviants. This outcome may partly reflect the smaller sample size compared to typical trichromats. Additionally, the high hit rates and low false alarm rates may indicate a ceiling effect, suggesting that both stimuli may not have been challenging enough to reveal more nuanced gradations in chromatic sensitivity. Alternatively, this ambivalence in RTs could reflect a potential post-receptoral enhancement, which may have mitigated the expected RT differences, particularly by facilitating RTs for red deviant to catch up with those for blue-green.

4.4.2 ERP Results

P3 amplitudes were expected to differ between stimulus conditions, reflecting attentional modulation driven by saliency differences. However, the LME model analysis did not reveal significant effects of chromatic sensitivity among participants. This may partly due to limited sample size, which was further impacted by the averaging process inherent in ERP analysis. Additionally, P3 reflects complex cognitive processes beyond saliency-driven attention modulation, introducing larger individual variations that obscured the expected effects.

Cluster-based permutation analysis provided further insights. For Typical trichromats, saliency-related neural differences were evident, with stronger and faster responses to the red deviant in the occipital to centro-parietal regions compared to the blue-green deviant. This aligns with the expectations based on their greater sensitivity to red-green contrast, compared to the categorically much similar blue-green and green contrast.

For anomalous trichromats, the faster neural response to the blue-green deviant was consistent with the expectation that this stimulus would be more salient for this group. However, contrary to previous studies suggesting robust post-receptoral modulation or clear neural compensation mechanisms (Rabin et al., 2018; Tregillus et al., 2021), no such pronounced differences in neural enhancement were observed. This highlights the need for further investigation into how perceptual processes differ across color vision types and how these are reflected in neural activity.

While both typical and anomalous trichromats demonstrated saliency-driven neural activity reflecting the reverse saliency relationship, the comparative analysis between color vision types, using cluster-based permutation analysis, did not reveal a clear distinction between the groups, contrary to the expectations.

One possible explanation is that, unlike behavioral analysis, ERP data require an averaging process, which can make the results more sensitive to random variation among participants, particularly when sample size is limited. Additionally, the varying chromatic sensitivity within each group may have introduced further individual variations, potentially masking any underlying differences in neural signals between the color vision types.

Overall, the attention-demanding paradigm used in this study effectively evoked neural activity across a broad spatiotemporal scale in different color vision types. In particular, the paradigm's ability to highlight temporal differences in perceived saliency among anomalous trichromats supports its utility in investigating perceptual diversity.

4.5 Limitation of the Study

While typical trichromats demonstrated saliency-oriented behavioral and neural responses, this effect was less clear in anomalous trichromats. This may be due to either insufficient saliency contrast between conditions or post-receptoral mechanisms that diminish the perceived contrast. Recent research (Lindsey et al., 2021) suggests that deuteranomalous trichromats require greater red-green contrast for effective perceptual differentiation, which supports the stimulus design based on red-green contrast. However, the stimuli may not have fully captured the neural processes compensating for reduced chromatic sensitivity in anomalous trichromats, limiting the ability to isolate clear neural markers for saliency differences.

Several factors likely contributed to this limitation. First, the small sample size, particularly for minority color vision phenotypes, reduced the statistical power, especially in ERP analysis where averaging was necessary. The combination of larger chromatic sensitivity and a small sample size made it more difficult to reflect this neural activity in statistical results.

Second, large individual differences in ERP waveforms, observed in both typical and anomalous trichromats, further complicated the interpretation of neural data. These waveform variations can be attributed to physiological differences, such as skull thickness (Hakim et al., 2021). Additionally, EEG primarily captures the activity of pyramidal neurons, while interneuron activity contributes minimally to the signal (Luck, 2014), which limits the signal's ability to reflect certain neural processes. Furthermore, attention-related neural signals are known to exhibit individual variability, contributing further complexities in interpretation (Curran et al., 2001; Kane and Engle, 2002). These inherent limitations of EEG may have obscured subtle neural differences related to chromatic sensitivity. To illustrate these individual differences in ERP waveforms, detailed results for each participant are provided in Appendix D.

Additionally, the study was unable to determine whether variations in red-green sensitivity were due to genetic factors or neuroplastic changes. This may have limited the ability to fully account for individual differences. Understanding these underlying factors—by disentangling genetic influences, such as inherent cone sensitivity, from developmental influences—and how these elements interact in individuals could help interpret neural signals more comprehensively and enhance the understanding of the diversity in perceptual and cognitive processes.

4.6 Concluding Remarks

This study aimed to provide insight into how variations in color vision types and chromatic sensitivity influence both behavioral and neural responses to color saliency, particularly when observing chromatically identical stimuli. While typical trichromats exhibited clear saliency-related patterns, the results for anomalous trichromats suggest a more complex interplay of factors, with potential involvement of compensatory mechanisms. By considering both

categorical and continuous variations in chromatic sensitivity, a more comprehensive view of individual differences in color perception was provided. However, further research with larger samples is necessary to fully elucidate the underlying neural mechanisms driving these variations.

References

Aine, C. J. and Harter, M. R. (1986). Visual event-related potentials to colored patterns and color names: Attention to features and dimension. *Electroencephalography and clinical Neurophysiology*, 64(3):228–245.

Alho, K., Woods, D. L., Algazi, A., and Näätänen, R. (1992). Intermodal selective attention. ii. effects of attentional load on processing of auditory and visual stimuli in central space. *Electroencephalography and clinical Neurophysiology*, 82(5):356–368.

Altman, N. and Krzywinski, M. (2016). Regression diagnostics: residual plots can be used to validate assumptions about the regression model. *Nature Methods*, 13(5):385–387.

Asenjo, A. B., Rim, J., and Oprian, D. D. (1994). Molecular determinants of human red/green color discrimination. *Neuron*, 12(5):1131–1138.

Barbur, J. L. and Rodriguez-Carmona, M. (2017). Colour vision requirements in visually demanding occupations. *British medical bulletin*, 122(1):51–77.

Barbur, J. L., Rodriguez-Carmona, M., and Evans, B. E. (2021). Color vision assessment-3. an efficient, two-step, color assessment protocol. *Color Research & Application*, 46(1):33–45.

Boehm, A. E., Bosten, J., and MacLeod, D. I. (2021). Color discrimination in anomalous trichromacy: Experiment and theory. *Vision Research*, 188:85–95.

Borges, R., Johnson, W. E., O'Brien, S. J., Gomes, C., Heesy, C. P., and Antunes, A. (2018). Adaptive genomic evolution of opsins reveals that early mammals flourished in nocturnal environments. *BMC genomics*, 19:1–12.

Bosten, J. (2019). The known unknowns of anomalous trichromacy. *Current Opinion in Behavioral Sciences*, 30:228–237.

Bowmaker, J. K. (1998). Evolution of colour vision in vertebrates. *Eye*, 12(3):541–547.

Brainard, D. H. and Vision, S. (1997). The psychophysics toolbox. *Spatial vision*, 10(4):433–436.

Broackes, J. (2010). Unilateral colour vision defects and the dimensions of dichromat experience. *Ophthalmic and Physiological Optics*, 30(5):672–684.

Bucci, P. and Galderisi, S. (2011). Physiologic basis of the EEG signal. *Standard electroencephalography in clinical psychiatry: A practical handbook*, pages 7–12.

Caine, N. G., Osorio, D., and Mundy, N. I. (2010). A foraging advantage for dichromatic marmosets (callithrix geoffroyi) at low light intensity. *Biology Letters*, 6(1):36–38.

Comerchero, M. D. and Polich, J. (1999). P3a and P3b from typical auditory and visual stimuli. *Clinical neurophysiology*, 110(1):24–30.

Conway, B. R. (2018). The organization and operation of inferior temporal cortex. *Annual review of vision science*, 4(1):381–402.

Cook, R. D. (1979). Influential observations in linear regression. *Journal of the American Statistical Association*, 74(365):169–174.

Curran, T., Hills, A., Patterson, M. B., and Strauss, M. E. (2001). Effects of aging on visuospatial attention: an ERP study. *Neuropsychologia*, 39(3):288–301.

Darlington, R. B. and Hayes, A. F. (2016). *Regression analysis and linear models: Concepts, applications, and implementation*. Guilford Publications.

Deeb, S. (2005). The molecular basis of variation in human color vision. *Clinical genetics*, 67(5):369–377.

Delorme, A. (2021). Clean rawdata version 2.0. *Vol., ed.ˆ eds*.

Delorme, A. (2023). EEG is better left alone. *Scientific reports*, 13(1):2372.

Delorme, A. and Makeig, S. (2004). EEGLAB: an open source toolbox for analysis of single-trial EEG dynamics including independent component analysis. *Journal of neuroscience methods*, 134(1):9–21.

Denison, R. N., Vu, A. T., Yacoub, E., Feinberg, D. A., and Silver, M. A. (2014). Functional mapping of the magnocellular and parvocellular subdivisions of human lgn. *Neuroimage*, 102:358–369.

Donchin, E. and Coles, M. G. (1988). Is the P300 component a manifestation of context updating? *Behavioral and brain sciences*, 11(3):357–374.

Donchin, E., Spencer, K. M., and Dien, J. (1997). The varieties of deviant experience: ERP manifestations of deviance processors.

Eimer, M. (1997). An event-related potential (ERP) study of transient and sustained visual attention to color and form. *Biological Psychology*, 44(3):143–160.

Fairman, H. S., Brill, M. H., and Hemmendinger, H. (1997). How the cie 1931 color-matching functions were derived from wright-guild data. *Color Research & Application: Endorsed by Inter-Society Color Council, The Colour Group (Great Britain), Canadian Society for Color, Color Science Association of Japan, Dutch Society for the Study of Color, The Swedish Colour Centre Foundation, Colour Society of Australia, Centre Français de la Couleur*, 22(1):11–23.

Fang, F. and He, S. (2005). Cortical responses to invisible objects in the human dorsal and ventral pathways. *Nature neuroscience*, 8(10):1380–1385.

Gefen, D. (2004). What makes an ERP implementation relationship worthwhile: Linking trust mechanisms and ERP usefulness. *Journal of Management Information Systems*, 21(1):263–288.

Glazer, J. E., Kelley, N. J., Pornpattananangkul, N., Mittal, V. A., and Nusslock, R. (2018). Beyond the frn: Broadening the time-course of EEG and ERP components implicated in reward processing. *International Journal of Psychophysiology*, 132:184–202.

Gorgolewski, K. J., Auer, T., Calhoun, V. D., Craddock, R. C., Das, S., Duff, E. P., Flandin, G., Ghosh, S. S., Glatard, T., Halchenko, Y. O., et al. (2016). The brain imaging data structure, a format for organizing and describing outputs of neuroimaging experiments. *Scientific data*, 3(1):1–9.

Grasso, D. J., Moser, J. S., Dozier, M., and Simons, R. (2009). ERP correlates of attention allocation in mothers processing faces of their children. *Biological Psychology*, 81(2):95–102.

Hakim, N., Awh, E., Vogel, E. K., and Rosenberg, M. D. (2021). Inter-electrode correlations measured with EEG predict individual differences in cognitive ability. *Current Biology*, 31(22):4998–5008.

Harrison, X. A., Donaldson, L., Correa-Cano, M. E., Evans, J., Fisher, D. N., Goodwin, C. E., Robinson, B. S., Hodgson, D. J., and Inger, R. (2018). A brief introduction to mixed effects modelling and multi-model inference in ecology. *PeerJ*, 6:e4794.

Harter and Aine (1984). Brain mechanisms of visual selective attention. *Varieties of attention*.

Hillyard, S. A. and Münte, T. F. (1984). Selective attention to color and location: An analysis with event-related brain potentials. *Perception & psychophysics*, 36(2):185–198.

Hiramatsu, C., Melin, A. D., Allen, W. L., Dubuc, C., and Higham, J. P. (2017). Experimental evidence that primate trichromacy is well suited for detecting primate social colour signals. *Proceedings of the Royal Society B: Biological Sciences*, 284(1856):20162458.

Hiramatsu, C., Melin, A. D., Aureli, F., Schaffner, C. M., Vorobyev, M., and Kawamura, S. (2009). Interplay of olfaction and vision in fruit foraging of spider monkeys. *Animal Behaviour*, 77(6):1421–1426.

Holmes, A., Franklin, A., Clifford, A., and Davies, I. (2009). Neurophysiological evidence for categorical perception of color. *Brain and cognition*, 69(2):426–434.

Hubel, D. H. and Wiesel, T. N. (1977). Ferrier lecture-functional architecture of macaque monkey visual cortex. *Proceedings of the Royal Society of London. Series B. Biological Sciences*, 198(1130):1–59.

Hunt, D. M., Dulai, K. S., Cowing, J. A., Julliot, C., Mollon, J. D., Bowmaker, J. K., Li, W.-H., and Hewett-Emmett, D. (1998). Molecular evolution of trichromacy in primates. *Vision research*, 38(21):3299–3306.

Hunt, R. W. and Pointer, M. (1985). A colour-appearance transform for the cie 1931 standard colorimetric observer. *Color Research & Application*, 10(3):165–179.

Ingle, D. J., Goodale, M. A., Mansfield, R. J., et al. (1982). *Analysis of visual behavior*. Mit Press Cambridge, MA.

Isbell, J. R. (1964). *Uniform spaces*. Number 12. American Mathematical Soc.

Isreal, J. B., Wickens, C. D., and Donchin, E. (1980). The dynamics of P300 during dual-task performance. *Progress in brain research*, 54:416–421.

Jacobs, G. H. (2009). Evolution of colour vision in mammals. *Philosophical Transactions of the Royal Society B: Biological Sciences*, 364(1531):2957–2967.

Jacobs, G. H. (2012). The evolution of vertebrate color vision. *Sensing in nature*, pages 156–172.

Jameson, K. A., Winkler, A. D., Herrera, C., and Goldfarb, K. (2014). The veridicality of color: A case study of potential human tetrachromacy. *Technical Report Series MBS 14-02. Institute for Mathematical Behavioral Sciences University of California at Irvine. Irvine, CA, USA*.

Janáky, M., Borbély, J., Benedek, G., Kocsis, B. P., and Braunitzer, G. (2014). Achromatic luminance contrast sensitivity in x-linked color-deficient observers: An addition to the debate. *Visual neuroscience*, 31(1):99–103.

Jordan, G., Deeb, S. S., Bosten, J. M., and Mollon, J. D. (2010). The dimensionality of color vision in carriers of anomalous trichromacy. *Journal of vision*, 10(8):12–12.

Jordan, G. and Mollon, J. (2019). Tetrachromacy: The mysterious case of extra-ordinary color vision. *Current Opinion in Behavioral Sciences*, 30:130–134.

Kaarna, A., Toivanen, P., and Kuparinen, T. (2002). Chromaticity difference from surfaces defined from macadam ellipses. In *Conference on Colour in Graphics, Imaging, and Vision*, volume 1, pages 206–211. Society of Imaging Science and Technology.

Kane, M. J. and Engle, R. W. (2002). The role of prefrontal cortex in working-memory capacity, executive attention, and general fluid intelligence: An individual-differences perspective. *Psychonomic bulletin & review*, 9(4):637–671.

Kaneko, S., Kuriki, I., and Andersen, S. K. (2020). Steady-state visual evoked potentials elicited from early visual cortex reflect both perceptual color space and cone-opponent mechanisms. *Cerebral Cortex Communications*, 1(1):tgaa059.

Kastner, S., Schneider, K. A., and Wunderlich, K. (2006). Beyond a relay nucleus: neuroimaging views on the human lgn. *Progress in brain research*, 155:125–143.

Kawamura, S. (2016). Color vision diversity and significance in primates inferred from genetic and field studies. *Genes & genomics*, 38(9):779–791.

Keil, A., Debener, S., Gratton, G., Junghöfer, M., Kappenman, E. S., Luck, S. J., Luu, P., Miller, G. A., and Yee, C. M. (2014). Committee report: publication guidelines and recommendations for studies using electroencephalography and magnetoencephalography. *Psychophysiology*, 51(1):1–21.

Kirschstein, T. and Köhling, R. (2009). What is the source of the EEG? *Clinical EEG and neuroscience*, 40(3):146–149.

Kleiner, M., Brainard, D., Pelli, D., Ingling, A., Murray, R., and Broussard, C. (2007). Whats new in psychtoolbox-3? *Perception*, 36(14):2007.

Kravitz, D. J., Saleem, K. S., Baker, C. I., Ungerleider, L. G., and Mishkin, M. (2013). The ventral visual pathway: an expanded neural framework for the processing of object quality. *Trends in cognitive sciences*, 17(1):26–49.

Kuniecki, M., Pilarczyk, J., and Wichary, S. (2015). The color red attracts attention in an emotional context. an ERP study. *Frontiers in human neuroscience*, 9:212.

Kurtenbach, A., Meierkord, S., and Kremers, J. (1999). Spectral sensitivities in dichromats and trichromats at mesopic retinal illuminances. *Journal of the Optical Society of America A*, 16(7):1541–1548.

Lamb, T. D., Collin, S. P., and Pugh, E. N. (2007). Evolution of the vertebrate eye: opsins, photoreceptors, retina and eye cup. *Nature Reviews Neuroscience*, 8(12):960–976.

Lee, B., Martin, P., and Valberg, A. (1988). The physiological basis of heterochromatic flicker photometry demonstrated in the ganglion cells of the macaque retina. *The Journal of physiology*, 404(1):323–347.

Li, P., Garg, A. K., Zhang, L. A., Rashid, M. S., and Callaway, E. M. (2022). Cone opponent functional domains in primary visual cortex combine signals for color appearance mechanisms. *Nature Communications*, 13(1):6344.

Lindsey, D. T., Brown, A. M., and Hutchinson, L. N. (2021). Appearance of special colors in deuteranomalous trichromacy. *Vision research*, 185:77–87.

Liu, J. and Wandell, B. A. (2005). Specializations for chromatic and temporal signals in human visual cortex. *Journal of Neuroscience*, 25(13):3459–3468.

Luck, S. J. (2014). *An introduction to the event-related potential technique*. MIT press.

MacAdam, D. L. (1942). Projective transformations of color-mixture diagrams. *Journal of the Optical Society of America*, 32(1):2–6.

Mahy, M., Van Eycken, L., and Oosterlinck, A. (1994). Evaluation of uniform color spaces developed after the adoption of cielab and cieluv. *Color Research & Application*, 19(2):105–121.

Maris, E. and Oostenveld, R. (2007). Nonparametric statistical testing of EEG-and MEG-data. *Journal of neuroscience methods*, 164(1):177–190.

Maunsell, J. H., Ghose, G. M., Assad, J. A., Mcadams, C. J., Boudreau, C. E., and Noerager, B. D. (1999). Visual response latencies of magnocellular and parvocellular lgn neurons in macaque monkeys. *Visual neuroscience*, 16(1):1–14.

Mccarthy, G., Luby, M., Gore, J., and Goldman-Rakic, P. (1997). Infrequent events transiently activate human prefrontal and parietal cortex as measured by functional MRI. *Journal of neurophysiology*, 77(3):1630–1634.

Melamud, A., Hagstrom, S., and Traboulsi, E. (2004). Color vision testing. *Ophthalmic Genetics*, 25(3):159–187.

Melgosa, M., Hita, E., Romero, J., and del Barco, L. J. (1994). Color-discrimination thresholds translated from the cie (x, y, y) space to the cie 1976 (l*, a*, b*). *Color Research & Application*, 19(1):10–18.

Melin, A. D., Fedigan, L. M., Hiramatsu, C., Sendall, C. L., and Kawamura, S. (2007). Effects of colour vision phenotype on insect capture by a free-ranging population of white-faced capuchins, cebus capucinus. *Animal Behaviour*, 73(1):205–214.

Melin, A. D., Hiramatsu, C., Parr, N., Matsushita, Y., Kawamura, S., and Fedigan, L. M. (2014). The behavioral ecology of color vision: considering fruit conspicuity, detection distance and dietary importance. *International Journal of Primatology*, 35:258–287.

Merbs, S. L. and Nathans, J. (1992). Absorption spectra of the hybrid pigments responsible for anomalous color vision. *Science*, 258(5081):464–466.

Mishkin, M., Ungerleider, L. G., and Macko, K. A. (1983). Object vision and spatial vision: two cortical pathways. *Trends in neurosciences*, 6:414–417.

Miyakoshi, A. M. and Makeig, S. (2022). Cleanrawdata EEGLAB plugin.

Mokrzycki, W. and Tatol, M. (2011). Colour difference delta E—A survey. *Machine Graphics and Vision*, 20(4):383–411.

Mollon, J. D. (1989). "tho'she kneel'd in that place where they grew..." the uses and origins of primate colour vision. *Journal of Experimental Biology*, 146(1):21–38.

Montag, E. D. (1994). Surface color naming in dichromats. *Vision Research*, 34(16):2137–2151.

Montag, E. D. and Boynton, R. M. (1987). Rod influence in dichromatic surface color perception. *Vision Research*, 27(12):2153–2162.

Moreira, H., Lillo, J., and Álvaro, L. (2021). "red-green" or "brown-green" dichromats? the accuracy of dichromat basic color terms metacognition supports denomination change. *Frontiers in Psychology*, 12:624792.

Morgan, M. J., Adam, A., and Mollon, J. D. (1992). Dichromats detect colour-camouflaged objects that are not detected by trichromats. *Proceedings of the Royal Society of London. Series B: Biological Sciences*, 248(1323):291–295.

Mullen, K. T., Thompson, B., and Hess, R. F. (2010). Responses of the human visual cortex and LGN to achromatic and chromatic temporal modulations: an fMRI study. *Journal of vision*, 10(13):13–13.

Murray, M. M., Brunet, D., and Michel, C. M. (2008). Topographic ERP analyses: a step-by-step tutorial review. *Brain topography*, 20(4):249–264.

Näätänen, R. and Gaillard, A. (1983). 5 the orienting reflex and the n2 deflection of the event-related potential (ERP). In *Advances in psychology*, volume 10, pages 119–141. Elsevier.

Nagy, A. L. and Boynton, R. M. (1979). Large-field color naming of dichromats with rods bleached. *Journal of the Optical Society of America*, 69(9):1259–1265.

Namima, T., Yasuda, M., Banno, T., Okazawa, G., and Komatsu, H. (2014). Effects of luminance contrast on the color selectivity of neurons in the macaque area v4 and inferior temporal cortex. *Journal of Neuroscience*, 34(45):14934–14947.

Nathans, J., Piantanida, T. P., Eddy, R. L., Shows, T. B., and Hogness, D. S. (1986). Molecular genetics of inherited variation in human color vision. *Science*, 232(4747):203–210.

Neitz, J. and Neitz, M. (2011). The genetics of normal and defective color vision. *Vision research*, 51(7):633–651.

Neitz, J., Neitz, M., He, J., and Shevell, S. (1999). Trichromatic color vision with only two spectrally distinct photopigments. *nature neuroscience*, 2(10):884–888.

Ohno, Y. (2000). Cie fundamentals for color measurements. In *NIP & Digital Fabrication Conference*, volume 16, pages 540–545. Society of Imaging Science and Technology.

Oostenveld, R., Fries, P., Maris, E., and Schoffelen, J.-M. (2011). Fieldtrip: open source software for advanced analysis of MEG, EEG, and invasive electrophysiological data. *Computational intelligence and neuroscience*, 2011:1–9.

Oostenveld, R. and Praamstra, P. (2001). The five percent electrode system for high-resolution EEG and ERP measurements. *Clinical neurophysiology*, 112(4):713–719.

Pastilha, R. C., Linhares, J. M., Gomes, A. E., Santos, J. L., de Almeida, V. M., and Nascimento, S. M. (2019). The colors of natural scenes benefit dichromats. *Vision Research*, 158:40–48.

Pelli, D. G. and Vision, S. (1997). The videotoolbox software for visual psychophysics: Transforming numbers into movies. *Spatial vision*, 10:437–442.

Pernet, C. R., Appelhoff, S., Gorgolewski, K. J., Flandin, G., Phillips, C., Delorme, A., and Oostenveld, R. (2019). EEG-BIDS, an extension to the brain imaging data structure for electroencephalography. *Scientific data*, 6(1):103.

Picton, T. W. et al. (1992). The P300 wave of the human event-related potential. *Journal of clinical neurophysiology*, 9:456–456.

Picton, T. W., Lins, O. G., and Scherg, M. (1995). The recording and analysis of event-related potentials. *Handbook of neuropsychology*, 10:3–3.

Pion-Tonachini, L., Kreutz-Delgado, K., and Makeig, S. (2019). Iclabel: An automated electroencephalographic independent component classifier, dataset, and website. *NeuroImage*, 198:181–197.

Pointer, M. (1981). A comparison of the cie 1976 colour spaces. *Color Research & Application*, 6(2):108–118.

Pokorny, J., Smith, V. C., and Lutze, M. (1989). Heterochromatic modulation photometry. *Journal of the Optical Society of America A*, 6(10):1618–1623.

Polich, J. (1987). Task difficulty, probability, and inter-stimulus interval as determinants of P300 from auditory stimuli. *Electroencephalography and Clinical Neurophysiology/Evoked Potentials Section*, 68(4):311–320.

Potts, G. F. (2004). An ERP index of task relevance evaluation of visual stimuli. *Brain and cognition*, 56(1):5–13.

Pridmore, R. W. (2014). Orthogonal relations and color constancy in dichromatic colorblindness. *Plos One*, 9(9):e107035.

Rabin, J., Kryder, A., and Lam, D. (2018). Binocular facilitation of cone-specific visual evoked potentials in colour deficiency. *Clinical and Experimental Optometry*, 101(1):69–72.

Reinagel, P., Godwin, D., Sherman, S. M., and Koch, C. (1999). Encoding of visual information by lgn bursts. *Journal of neurophysiology*, 81(5):2558–2569.

Romero, R. and Polich, J. (1996). P3 (00) habituation from auditory and visual stimuli. *Physiology & behavior*, 59(3):517–522.

Rousselet, G. A., Thorpe, S. J., and Fabre-Thorpe, M. (2004). How parallel is visual processing in the ventral pathway? *Trends in cognitive sciences*, 8(8):363–370.

Sakurai, M. and Mullen, K. T. (2006). Cone weights for the two cone-opponent systems in peripheral vision and asymmetries of cone contrast sensitivity. *Vision research*, 46(26):4346–4354.

Sassenhagen, J. and Draschkow, D. (2019). Cluster-based permutation tests of MEG/EEG data do not establish significance of effect latency or location. *Psychophysiology*, 56(6):e13335.

Schanda, J. (2007). Cie colorimetry. *Colorimetry: Understanding the CIE system*, 3:25–78.

Schanda, J. (2016). *CIE u, v Uniform Chromaticity Scale Diagram and CIELUV Color Space*, pages 185–188. Springer New York, New York, NY.

Scheibner, H. M. and Boynton, R. M. (1968). Residual red-green discrimination in dichromats. *Journal of the Optical Society of America*, 58(8):1151–1158.

Sharpe, L. T., de Luca, E., Hansen, T., Jägle, H., and Gegenfurtner, K. R. (2006). Advantages and disadvantages of human dichromacy. *Journal of Vision*, 6(3):3–3.

Shaw, M. and Fairchild, M. (2002). Evaluating the 1931 cie color-matching functions. *Color Research & Application: Endorsed by Inter-Society Color Council, The Colour Group (Great Britain), Canadian Society for Color, Color Science Association of Japan, Dutch Society for the Study of Color, The Swedish Colour Centre Foundation, Colour Society of Australia, Centre Français de la Couleur*, 27(5):316–329.

Smith, T. and Guild, J. (1931). The cie colorimetric standards and their use. *Transactions of the optical society*, 33(3):73.

Smith, V. C. and Pokorny, J. (1977). Large-field trichromacy in protanopes and deuteranopes. *Journal of the Optical Society of America*, 67(2):213–220.

Stockman, A., MacLeod, D. I., and Johnson, N. E. (1993). Spectral sensitivities of the human cones. *Journal of the Optical Society of America A*, 10(12):2491–2521.

Stockman, A. and Sharpe, L. T. (2000). The spectral sensitivities of the middle-and long-wavelength-sensitive cones derived from measurements in observers of known genotype. *Vision research*, 40(13):1711–1737.

Sunaga, S., Ogura, T., and Seno, T. (2013). Evaluation of a dichromatic color-appearance simulation by a visual search task. *Optical review*, 20:83–93.

Sutton, S., Braren, M., Zubin, J., and John, E. (1965). Evoked-potential correlates of stimulus uncertainty. *Science*, 150(3700):1187–1188.

Tait, D. M. and Carroll, J. (2009). Normality of colour vision in a compound heterozygous female carrying protan and deutan defects. *Clinical and Experimental Optometry*, 92(4):356–361.

Thomas, P., Formankiewicz, M., and Mollon, J. (2011). The effect of photopigment optical density on the color vision of the anomalous trichromat. *Vision research*, 51(20):2224–2233.

Tregillus, K. E., Isherwood, Z. J., Vanston, J. E., Engel, S. A., MacLeod, D. I., Kuriki, I., and Webster, M. A. (2021). Color compensation in anomalous trichromats assessed with fMRI. *Current Biology*, 31(5):936–942.

Troscianko, J., Wilson-Aggarwal, J., Griffiths, D., Spottiswoode, C. N., and Stevens, M. (2017). Relative advantages of dichromatic and trichromatic color vision in camouflage breaking. *Behavioral Ecology*, 28(2):556–564.

Verriest, G., Van Laethem, J., and Uvijls, A. (1982). A new assessment of the normal ranges of the farnsworth-munsell 100-hue test scores. *American journal of ophthalmology*, 93(5):635–642.

Wandell, B. A. and Winawer, J. (2011). Imaging retinotopic maps in the human brain. *Vision research*, 51(7):718–737.

Witzel, C. and Gegenfurtner, K. R. (2015). Categorical facilitation with equally discriminable colors. *Journal of vision*, 15(8):22–22.

Wundheiler, A. W. (1945). On the macadam ellipses. *Journal of the Optical Society of America*, 35(12):767–770.

Xian-Guang, H., Aldridge, R. J., Siveter, D. J., Siveter, D. J., and Xiang-Hong, F. (2002). New evidence on the anatomy and phylogeny of the earliest vertebrates. *Proceedings of the Royal Society of London. Series B: Biological Sciences*, 269(1503):1865–1869.

Zapata-Saldarriaga, L.-M., Vargas-Serna, A.-D., Gil-Gutiérrez, J., Mantilla-Ramos, Y.-J., and Ochoa-Gómez, J.-F. (2023). Evaluation of strategies based on wavelet-ICA and IClabel for artifact correction in EEG recordings. *Revista científica*, (46):61–76.

Chapter A

Individual Results of Luminance Adjustment

Participant code	Color vision type	Mean luminance (cd/m^2)		
		Deviant 1	Deviant 2	Standard
Participant 01	Typical trichromacy	20.93	19.78	20.54
Participant 04	Typical trichromacy	20.93	19.23	19.23
Participant 05	Typical trichromacy	20.34	19.65	20.18
Participant 06	Typical trichromacy	20.46	20.15	19.96
Participant 08	Typical trichromacy	20.61	19.70	20.43
Participant 09	Typical trichromacy	20.04	20.28	20.13
Participant 10	Typical trichromacy	21.13	19.59	20.54
Participant 11	Typical trichromacy	20.45	19.70	20.24
Participant 12	Tyical trichromacy	20.28	20.17	20.19
Participant 13	Typical trichromacy	20.39	19.54	20.33
Participant 15	Typical trichromacy	20.47	20.18	20.09
Participant 17	Typical trichromacy	19.83	19.09	19.23
Participant 19	Typical trichromacy	20.57	19.55	20.29

Table A.1 Individual stimuli luminance equated to 20 cd/m^2, as measured using the flicker photometry method, for participants with typical trichromacy. These luminance values were used during the oddball experiment.

Participant code	Color vision type	Mean luminance (cd/m^2)		
		Deviant 1	Deviant 2	Standard
Participant 02	Deuteranomalous trichromacy	21.28	18.93	20.67
Participant 03	Deuteranomalous trichromacy	21.17	19.08	20.60
Participant 07	Deuteranopia	21.43	19.04	20.77
Participant 14	Deuteranomalous trichromacy	21.34	18.90	20.66
Participant 16	Deuteranomalous trichromacy	21.35	19.08	20.43
Participant 18	Deuteranomalous trichromacy	21.18	18.83	20.62

Table A.2 Individual stimuli luminance equated to 20 cd/m^2, as measured using the flicker photometry method, for participants with minority color vision phenotypes (deuteranomalous trichromacy and deuteranopia). These luminance values were used during the oddball experiment.

Chapter B

Individual CAD test Results

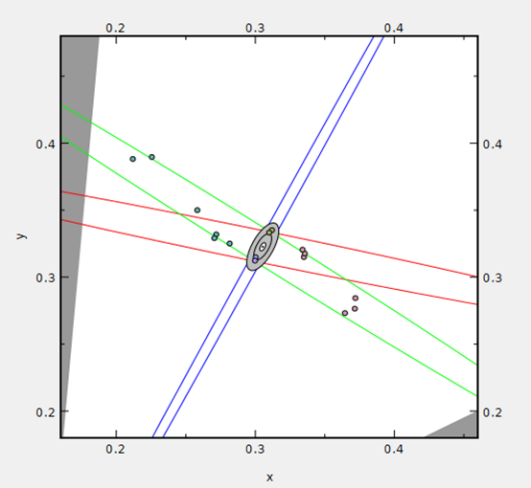

(a) CAD Test - Participant 02

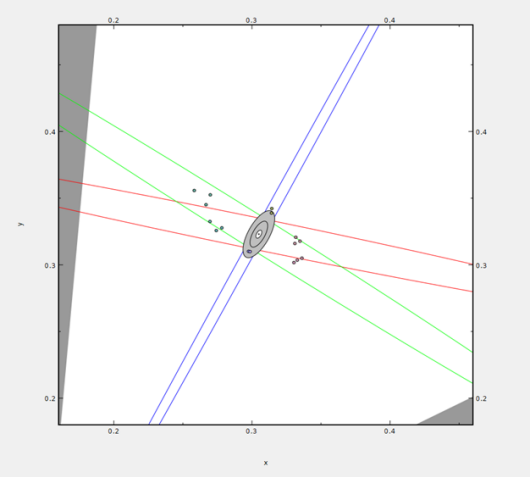

(b) CAD Test - Participant 03

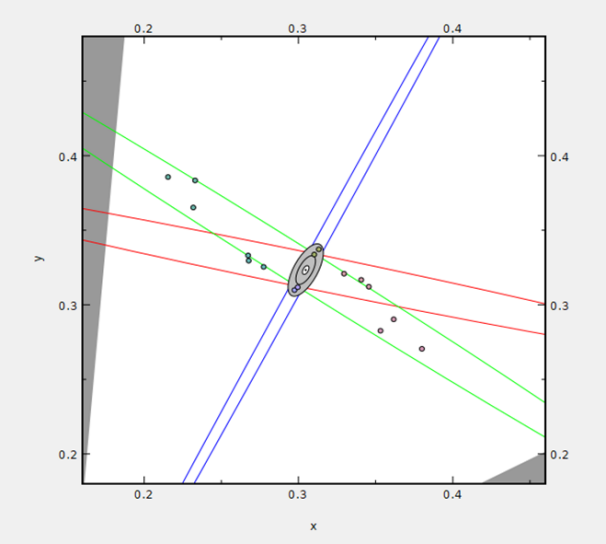

(c) CAD Test - Participant 07

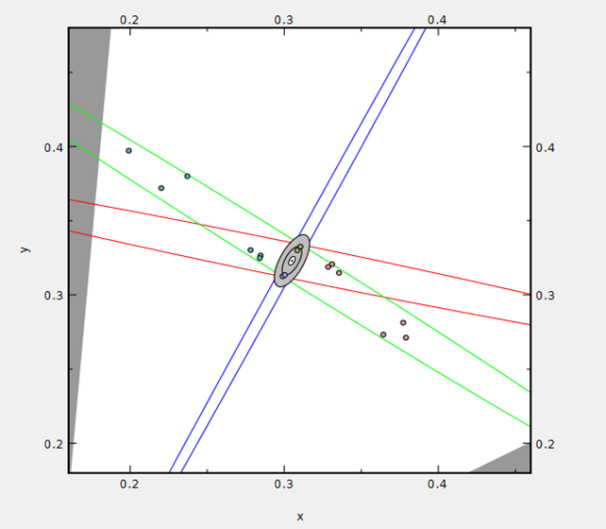

(d) CAD Test - Participant 14

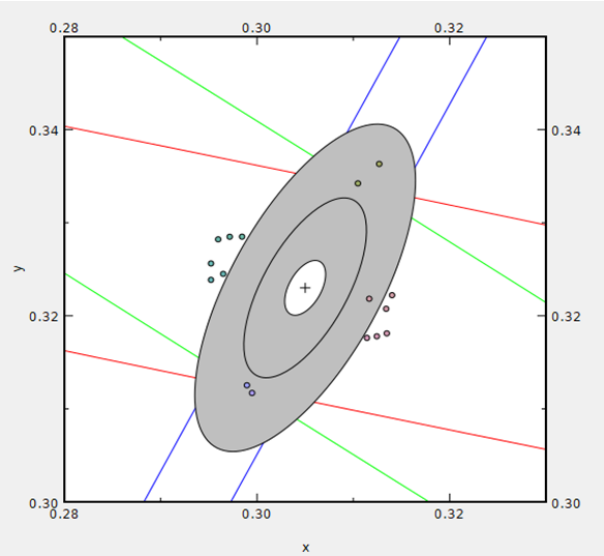

(e) CAD Test - Participant 16

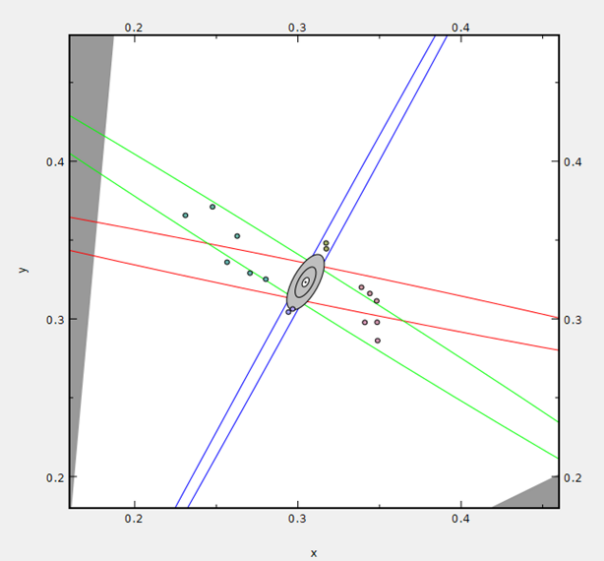

(f) CAD Test - Participant 18

Fig. B.1 Individual results of the CAD test for participants with minority color vision phenotypes. Each dot plotted in the CIE1931xy diagram corresponds to the discrimination threshold for the test stimuli. The inner circle in the gray area indicates the average discrimination threshold for typical trichromats, while the outer circle represents two standard deviations away from the average. Colored lines define the tested color axes within the diagram.

Chapter C

Individual Anomalo Scope Results

Result: Red/Green color vision

Eye:	Right
Date of exam.:	
Matching range:	Absolute
Duration:	18:58
Anomaly quotient	
AQ:	∞ to 0.30
Matching range	
Mixing light:	0.0 to 58.7
Reference light:	17.5 to 18.0
Assessment	
Not possible	
Comment	

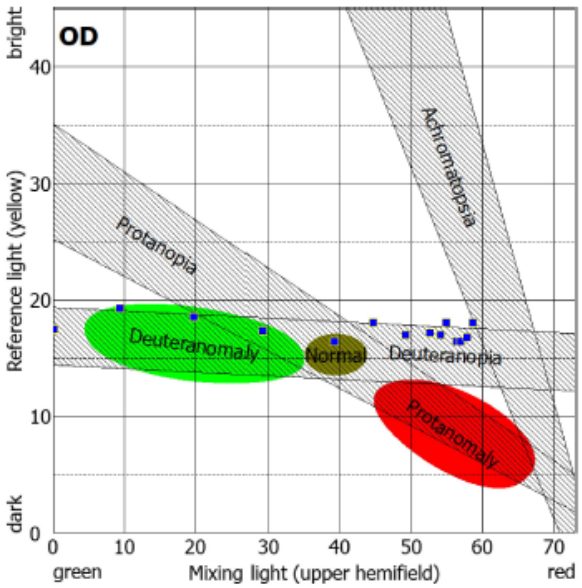

(a) Participant 02

Result: Red/Green color vision

Eye:	Right
Date of exam.:	
Matching range:	Absolute
Duration:	10:58
Anomaly quotient	
AQ:	50.30 to 2.04
Matching range	
Mixing light:	1.7 to 27.2
Reference light:	18.9 to 15.7
Assessment	
Not possible	
Comment	

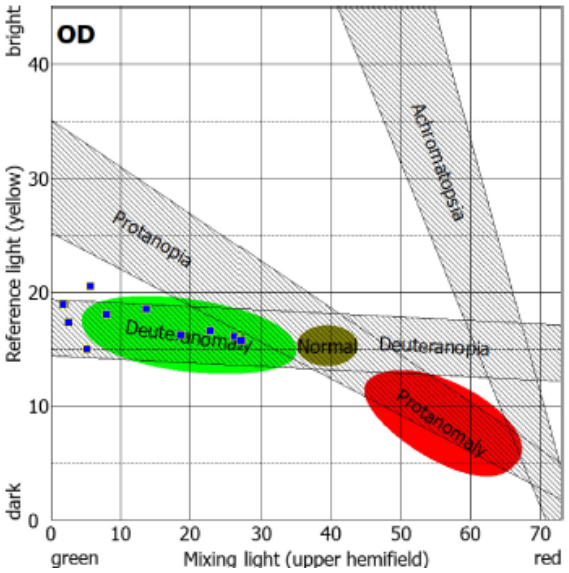

(b) Participant 03

Result: Red/Green color vision

Eye:	Right
Date of exam.:	
Matching range:	Absolute
Duration:	13:48
Anomaly quotient	
AQ:	307.88 to 0.01
Matching range	
Mixing light:	0.3 to 72.4
Reference light:	16.8 to 15.9
Assessment	
Deuteranopia	
Comment	

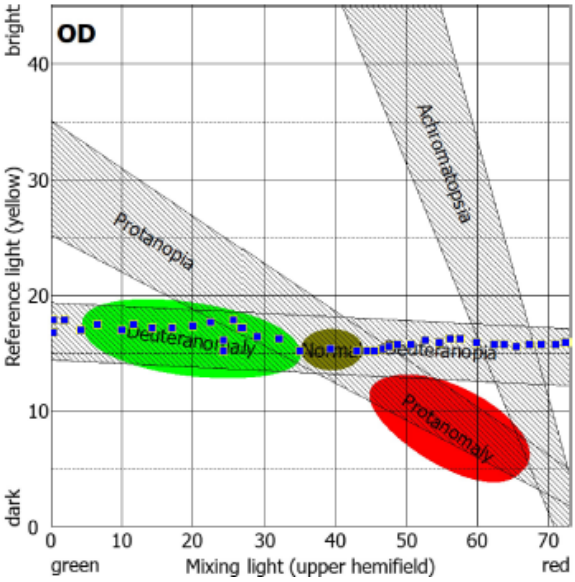

(c) Participant 07

Result: Red/Green color vision

Eye:	Right
Date of exam.:	
Matching range:	Absolute
Duration:	13:01
Anomaly quotient	
AQ:	3.47 to 0.78
Matching range	
Mixing light:	18.9 to 44.4
Reference light:	17.8 to 13.8
Assessment	
Deuteranomaly	
Comment	

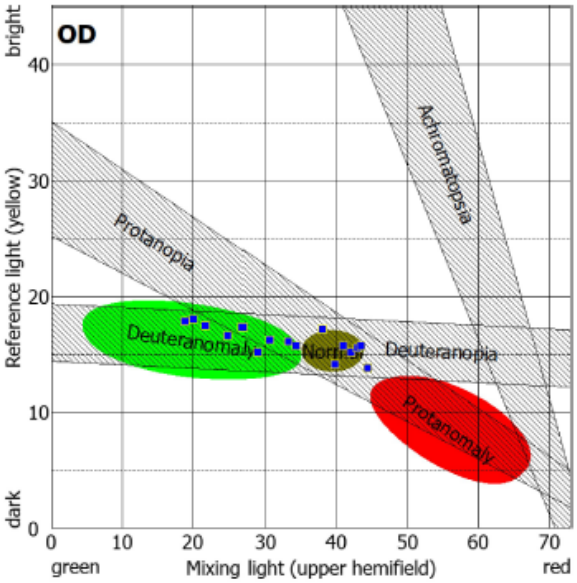

(d) Participant 14

Result: Red/Green color vision

Eye:	Right
Date of exam.:	
Matching range:	Absolute
Duration:	17:42
Anomaly quotient	
AQ:	3.33 to 2.01
Matching range	
Mixing light:	19.5 to 27.5
Reference light:	18.4 to 15.9
Assessment	
Deuteranomaly	
Comment	

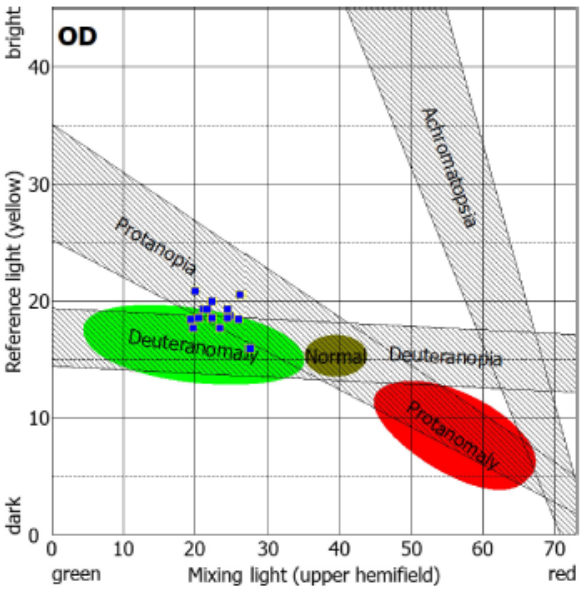

(e) Participant 16

Result: Red/Green color vision

Eye:	Right
Date of exam.:	
Matching range:	Absolute
Duration:	24:55
Anomaly quotient	
AQ:	4.12 to 3.02
Matching range	
Mixing light:	16.6 to 20.9
Reference light:	16.9 to 16.9
Assessment	
Deuteranomaly	
Comment	
Right eye result	

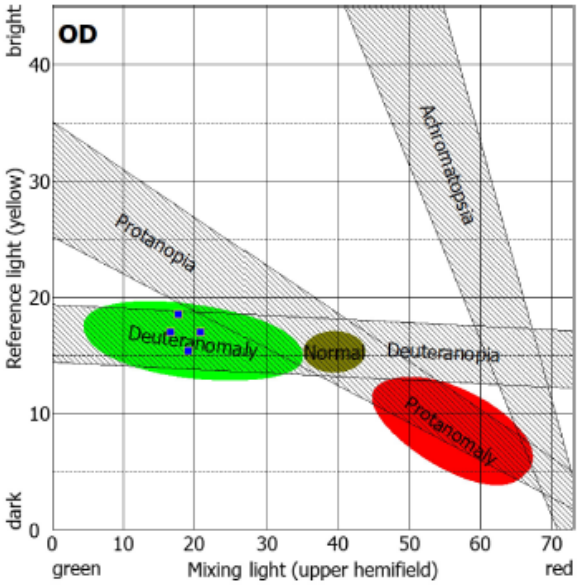

(f) Participant 18

Fig. C.1 Anomaloscope test results for individual participants with minority phenotypes (right eye results). The anomaloscope was used to differentiate color vision types between trichromacy and dichromacy in this study. For example, as shown for Participant 07 in (c), dichromats perceive a color match to monochromatic yellow at any red-green mixing ratio, indicating an absence or minimal function of the red-green opponency mechanism. This suggests that either the L or M cone is missing in the retina.

Chapter D

Individual RTs in Relation to Red-Green Sensitivities

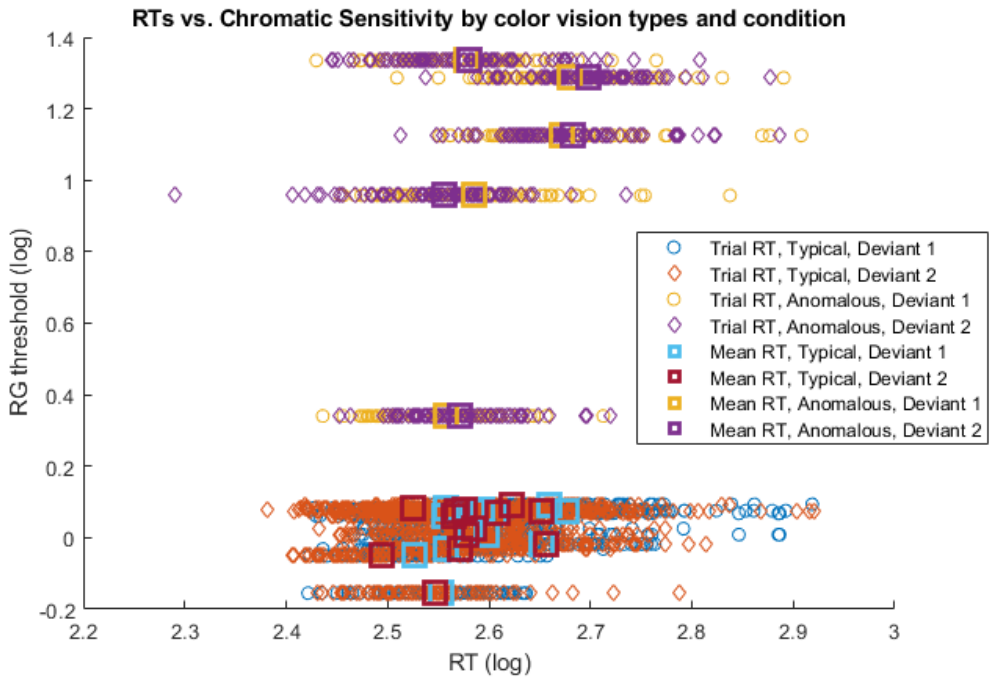

Fig. D.1 RT distribution relative to red-green threshold (RGtrheshold), representing chromatic sensitivity, for both deviant stimulus conditions (deviant 1: blue-green, deviant 2: red) across color vision types. RTs and RGtheshold are log-transformed.

Chapter E

Individual ERP plots

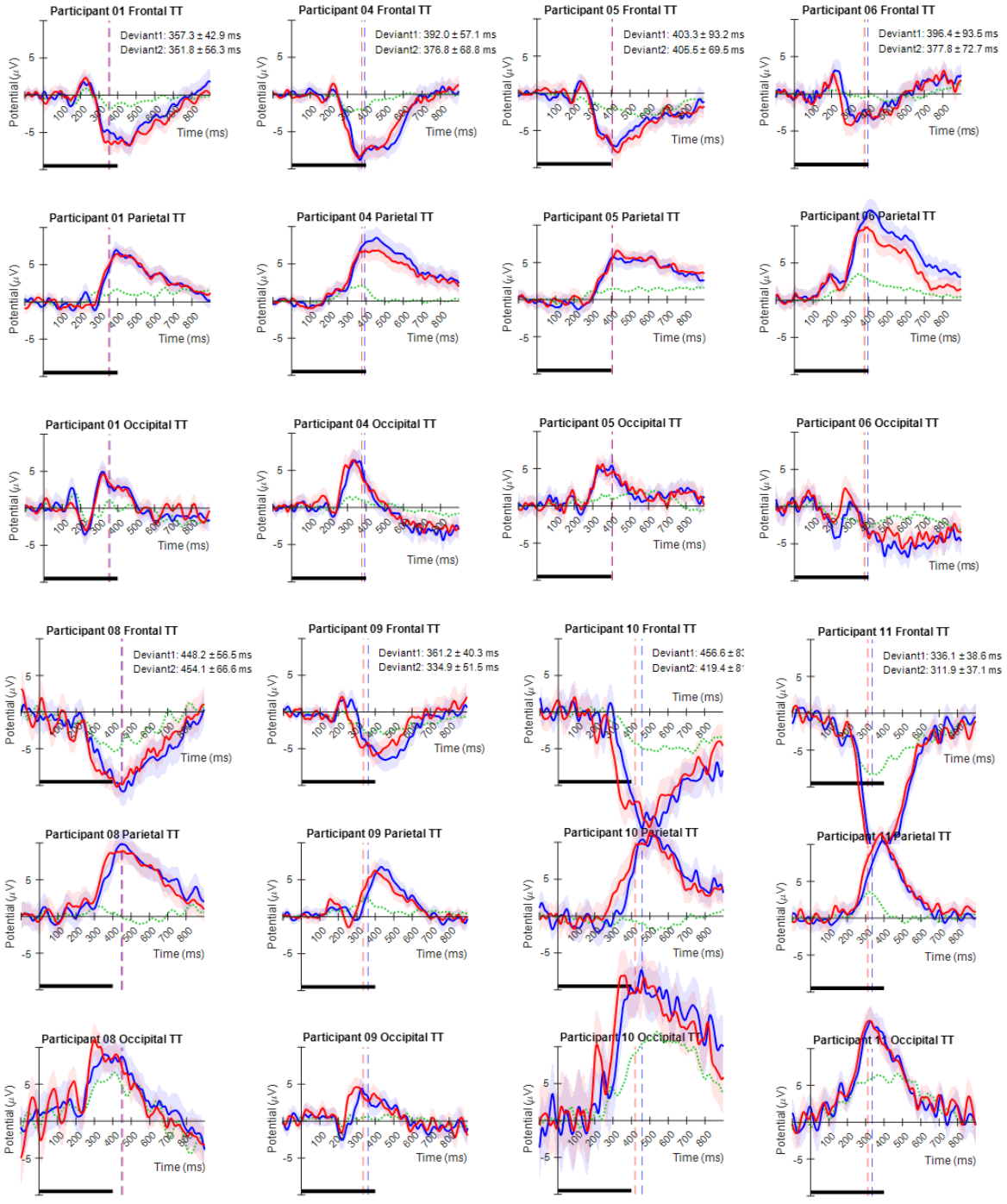
Participant 01 Frontal TT
Deviant1: 357.3 ± 42.9 ms
Deviant2: 351.8 ± 56.3 ms
Participant 04 Frontal TT
Deviant1: 392.0 ± 57.1 ms
Deviant2: 376.8 ± 68.8 ms
Participant 05 Frontal TT
Deviant1: 403.3 ± 93.2 ms
Deviant2: 405.5 ± 69.5 ms
Participant 06 Frontal TT
Deviant1: 396.4 ± 93.5 ms
Deviant2: 377.8 ± 72.7 ms
Participant 01 Parietal TT
Participant 04 Parietal TT
Participant 05 Parietal TT
Participant 06 Parietal TT
Participant 01 Occipital TT
Participant 04 Occipital TT
Participant 05 Occipital TT
Participant 06 Occipital TT
Participant 08 Frontal TT
Deviant1: 448.2 ± 56.5 ms
Deviant2: 454.1 ± 66.6 ms
Participant 09 Frontal TT
Deviant1: 361.2 ± 40.3 ms
Deviant2: 334.9 ± 51.6 ms
Participant 10 Frontal TT
Participant 11 Frontal TT
Deviant1: 336.1 ± 38.6 ms
Deviant2: 311.9 ± 37.1 ms
Participant 08 Parietal TT
Participant 09 Parietal TT
Participant 10 Parietal TT
Participant 11 Parietal TT
Participant 08 Occipital TT
Participant 09 Occipital TT
Participant 10 Occipital TT
Participant 11 Occipital TT
Potential (μV)
Time (ms)

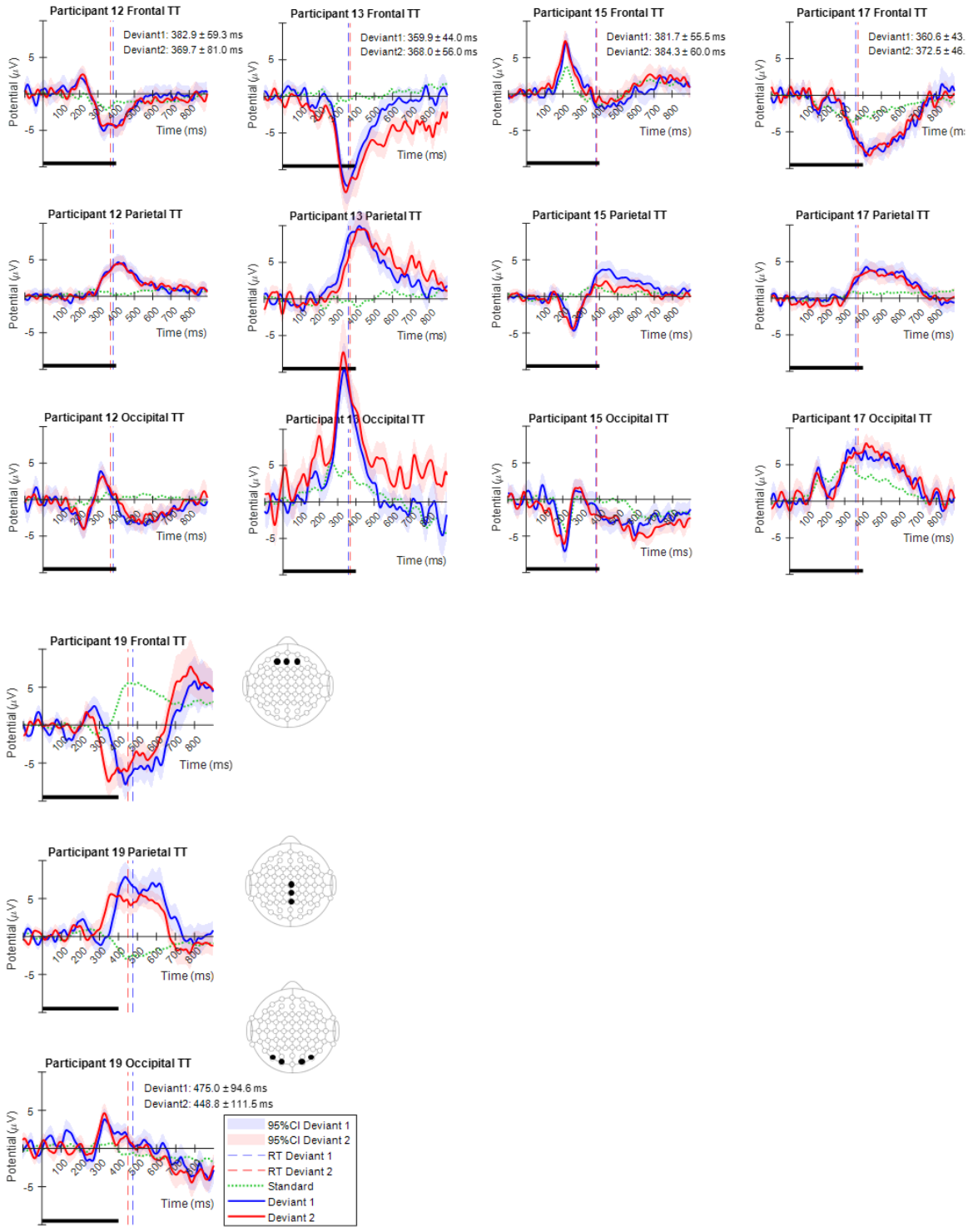

Fig. E.1 Individual ERPs from typical trichromats (TT). Post-preprocessed EEG data from the frontal, parietal, and occipital regions were averaged over trials for each individual. Averaged electrodes for each region correspond to AF3, AFz, AF4 in the frontal region, Cz, CPz, Pz in the parietal region, and PO7, O1, O2, PO8 in the occipital region. The mean and standard deviation of the RTs for each deviant stimulus are indicated as text inside the plot. Stimulus colors correspond as follows: Deviant 1: blue-green, Deviant 2: red, and Standard: green. The thick black line at the bottom indicates the stimuli presentation period.

Fig. E.2 Individual ERPs from anomalous trichromats (AT) and deuteranopic dichromats (D). Post-preprocessed EEG data from the frontal, parietal, and occipital regions were averaged over trials for each individual. The averaged electrodes for each region correspond to AF3, AFz, AF4 in the frontal region, Cz, CPz, Pz in the parietal region, and PO7, O1, O2, PO8 in the occipital region. The mean and standard deviation of the RTs for each deviant stimulus are indicated as text inside the plot. Stimulus colors correspond as follows: Deviant 1: blue-green, Deviant 2: red, and Standard: green. The thick black line at the bottom indicates stimuli presentation period. Participant number 07 had deuteranopic dichromacy, while the rest had anomalous trichromacy (all are deuteranomalous trichromacy).

Chapter F

Participant Instructions

作成日：2021/09/13

オドボール実験　教示

ディスプレイの中央にいくつかの色相をもつ、円盤状の刺激が呈示されます。

刺激の色相は、3 種類あります。色相よって、呈示される頻度が異なり、高頻度で呈示されるものと、低頻度で呈示されるものがあります。ディスプレイに低頻度で出現する色相の刺激が呈示されたら、できるだけ素早く、ボタンを押して応答してください。

実験は 10 回の連続した刺激呈示を 1 セッションとし、全部で 40 セッション行う実験を 2 度行います。時折呈示される低頻度の刺激は、1 セッション中、1 種類以上は含まれません。

セッション間には、休憩を挟みます。目が疲れた時など、適宜十分な休憩を取ってください。取り付けた電極に注意しながら、ストレッチをしても構いません。1 セッション中の 20 秒ほどは、ディスプレイ中央に視線を向け、集中して取り組むことが、重要となっています。

実験の刺激に慣れるため、本試行と同じ刺激を使った練習試行を行います。練習試行では刺激を観察して頂き、本番同様に低頻度の刺激に対してボタンを押す操作を行ってください。刺激とボタンの操作に十分慣れた後、本実験に移ります。

2021/09/13 作成

フリッカーフォトメトリー教示

画面の中央に 2 色の円盤が交互に表れる刺激が呈示されます。キーボードの 8（または、上矢印）を押すと、一つの色相の円盤の色が明るくなり、2（または、下矢印）を押すと暗くなります。キーボードを操作して、明るさ（暗さ）を調整すると、交互に表れる刺激のちらつきが小さくなっていきます。

ちらつきが最小になるところを見つけたら、エンターキーを押してちらつきが最小になる明るさを決定してください。

刺激は全部で 3 種類あり、各刺激、6 回ずつ行っていただきます。

※この実験では脳波は計測しません。